Ozone production and transport over the Amazon Basin during the dry-to-wet and wet-to-dry transition seasons

M. M. Bela[1,*], K. M. Longo[2], S. R. Freitas[2], D. S. Moreira[2], V. Beck[3], S. C. Wofsy[4], C. Gerbig[3], K. Wiedemann[4], M. O. Andreae[5], P. Artaxo[6]

[1] Center for Earth System Science (CCST), National Institute for Space Research (INPE), São José dos Campos, Brazil

[2] Center for Weather Forecast and Climate Studies, National Institute for Space Research (INPE), Cachoeira Paulista, Brazil

[3] Max Planck Institute for Biogeochemistry, Jena, Germany

[4] Division of Engineering and Applied Science/Department of Earth and Planetary Science, Harvard University, Cambridge, MA, USA

[5] Biogeochemistry Department, Max Planck Institute for Chemistry, Mainz, Germany

[6] Institute of Physics, University of São Paulo, São Paulo, Brazil

[*] Now at Laboratory for Atmospheric and Space Physics, University of Colorado, Boulder, USA

Correspondence to: M. M. Bela (megan.bela@colorado.edu)

Abstract

The Regional Carbon Balance in Amazonia (BARCA) campaign provided the first Amazon Basin-wide aircraft measurements of O_3 during both the dry-to-wet (November and December 2008) and wet-to-dry (May 2009) transition seasons. Extremely low background values (< 20 ppb) were observed to the west and north of Manaus in both seasons and in all regions during the wet-to-dry transition. On the other hand, elevated O_3 levels (40-60 ppb) were seen during the dry-to-wet transition to the east and south of Manaus, where biomass burning emissions of O_3 precursors were present. Chemistry simulations with the CCATT-BRAMS and WRF-Chem models are within the error bars of the observed O_3 profiles in the boundary layer (0-3 km a.s.l.) in polluted conditions. However, the models overestimate O_3 in the boundary layer in clean conditions, despite lacking the predominant NO source from soil. In addition, O_3 simulated by the models was either within the error bars or lower than BARCA observations in midlevels (3–5 km a.s.l.), and lower than total tropospheric O_3 retrieved from OMI/MLS, which is primarily comprised of middle troposphere O_3 and thus reflects long-range transport processes. Therefore, the models do a relatively poor job of representing the free troposphere-BL gradient in O_3 compared with aircraft and satellite observations, which could be due to missing long-range and convective transport of O_3 at mid-levels. Additional simulations with WRF-Chem showed that the model O_3 production is very sensitive to both the O_3 deposition velocities and the NO_x emissions, which were both about one half of observed values. These results indicate the necessity of more realistic model representations of emissions, deposition and convective processes for accurate monitoring and prediction of increases in O_3 production in the Amazon Basin as the regional population grows.

1 Introduction

In the Amazon Basin, trace gases from biomass-burning, urban, and biogenic emissions are important sources of ozone precursors, which are efficiently transported by intense convective activity to the upper troposphere, where they can be dispersed over long distances by regional and global circulations. Additionally, convective overshooting may inject heat, moisture and trace gases into the tropical tropopause layer, impacting stratospheric ozone and other aspects of global climate (Fueglistaler et al., 2009). In the dry-to-wet transition season, regional smoke and haze plumes from biomass burning are observed (Longo et al., 2009). On the other hand, in the wet-to-dry transition season, biogenic emission of VOCs, particularly from the Amazon rainforest, may maintain the atmospheric oxidative capacity for generating ozone and other photochemical pollutants (Lelieveld et al., 2008).

The Amazon Basin continues to rapidly urbanize, and urban emissions of O_3 precursors are also expected to grow. Emissions from cities in the tropics may have a larger impact on the upper troposphere due to high solar radiation levels and intense convective transport (Gallardo et al., 2010). In the upper troposphere, O_3 acts as a greenhouse gas, increasing surface radiative forcing (IPCC, 2001). Inhalation of elevated levels of ozone can irritate the lungs, aggravate asthma and cause emphysema, bronchitis, and premature death (Schwela, 2000). High ozone concentrations can also inhibit photosynthesis in plants and damage leaf tissue, harming wild ecosystems and reducing crop productivity (Reich and Amundson, 1985). Thus, an improved understanding and quantification of O_3 temporal and spatial variability in the tropical rainforest environment is important for projecting future impacts of land use and climate change in the Amazon Basin and other tropical rainforest regions worldwide on their expanding human populations and significant biodiversity.

Analyses of satellite, aircraft and ground-based observations of O_3 over Amazonia since the 1980s have demonstrated the influence of long-range transport of African biomass burning and Northern Hemisphere inputs, local fire sources, NO soil and biogenic VOC emissions, and convective transport on spatial and seasonal variability in O_3. In particular, data from the ABLE-2B aircraft and ground campaign during the 1987 wet-to-dry transition season and the BARCA observations offer the opportunity to compare the regional O_3 distribution across decades.

Previous analyses of satellite ozone data have noted early-year O_3 maximums in tropical Southern Hemisphere primarily associated with cross-Atlantic transport of biomass burning emissions from Africa (Fishman and Larson, 1987; Thompson et al., 1996), Northern Hemisphere fires, and lightning NO_x (Edwards et al., 2003). In the Amazon region, ground-based and aircraft campaigns (e.g., Crutzen et al., 1985; Kirchhoff et al., 1990; Browell et al., 1996; Kaufman et al., 1998; Longo et al., 1999, Andreae et al., 2001; Andreae et al., 2002; Zhou et al., 2002; Cordova et al., 2003; Rummel et al., 2007; Kuhn et al., 2010; Martin et al., 2010; Toon et al., 2010) have observed daytime background O_3 levels of 10-20 ppb, decreasing to very low values (~5 ppb) at night due to O_3 deposition to the forest. However, nighttime values can be increased up to 30 ppb due to convective downdrafts (Betts et al., 2002; Cordova et al., 2003). Elevated levels of 60-80 ppb are found due to production from regional fire emissions and recirculated urban pollution from SE Brazil, as well as evidence of deep convective transport of boundary layer air to the middle and upper troposphere.

Thus, satellite observations enable the attribution of tropical O_3 maxima to biomass burning and lightning NO_x sources, while ground-based measurements allow the identification of key surface processes in the Amazon Basin affecting O_3 amounts. These processes include O_3 production from soil NO_x emissions and removal via dry deposition to the forest canopy. Aircraft campaigns complete the suite of observations, allowing the examination of convective lofting of surface emissions, with biomass burning emissions of particular importance on the regional scale. In-situ data on cloud properties and chemical species, as well as observations of land use changes, boundary layer dynamics and larger-scale cloud-aerosol interactions, are scant in this region. Therefore, models are essential tools for monitoring and predicting atmospheric chemistry composition, weather, and climate at local, regional and global scales. In turn, the observations help constrain uncertainties in the model representations of parameterized convection, turbulence, land surface and other subgrid scale processes that affect the simulated transport and chemical transformation of the atmospheric composition (Beck et al., 2013).

Motivated by the impact of O_3 in the Amazon Basin on human and ecosystem health and global climate, we collected aircraft observations of O_3 during BARCA and conducted regional chemistry simulations in order to answer the following scientific questions: how does O_3 vary spatially and seasonally over the Amazon basin? What are the sources and sinks of O_3 in this region? How well can state-of-the-art regional chemistry models reproduce O_3 distributions over the Amazon Basin?

The structure of this paper is as follows. In Section 2, the measurements taken during the BARCA aircraft campaign are presented, followed by the meteorological conditions and emissions regimes during the two phases of the campaign. The ABLE-2 campaigns from the 1980s are also described in this section. Sections 3.1-3.3 detail the aircraft observations, the setup of the CCATT-BRAMS and WRF-Chem simulations and the ground-based and remote sensing observations used in the analysis. In Section 4.1, the O_3 aircraft observations are presented, followed by the analysis of observed and modeled transition season meteorology in Section 4.2 and the findings from the O_3

simulations and process studies in Section 4.3. Final discussions and conclusions are found in Section 5.

2 BARCA aircraft campaigns

The Regional Carbon Balance in Amazonia (BARCA) Large-Scale Biosphere-Atmosphere (LBA) experiment was an aircraft campaign based in Manaus and conducted during the dry-to-wet (November and December 2008) and wet-to-dry (May 2009) transition seasons. BARCA was the first flight campaign to sample ozone and other trace gases on a regional scale in both transition seasons. It offers a unique opportunity, together with satellite observations and modeling studies, to understand the regional ozone distribution in the Amazon under different meteorological and emissions regimes.

The BARCA flights were conducted with the EMB 110 Bandeirante aircraft of the Brazilian National Institute for Space Research (INPE). In-situ measurements were made of carbon dioxide (CO_2), carbon monoxide (CO), methane (CH_4), ozone (O_3), and aerosol number concentration and optical properties. Flask samples were collected to determine CO_2, CH_4, sulfur hexafluoride (SF_6), CO, nitrous oxide (N_2O), hydrogen, and the oxygen-nitrogen ratio (O_2/N_2). The flights consisted of quasi-Lagrangian measurements, which attempt to sample an air parcel at multiple locations along its path in order to constrain regional and basin-wide fluxes of these species. The aircraft had a ceiling of 4500 m, and flights usually consisted of ascending and descending vertical profiles separated by short (5-30 min) horizontal legs. A detailed description of the aircraft measurements can be found in Andreae et al. (2012). Figure 1 shows a map of the flight tracks from BARCA A and B. Both experiment periods included flights to the north, south and east of Manaus, as well as local flights near Manaus. Only BARCA A included flights to the west of Manaus, because intense convective activity in that region during BARCA B precluded flying. During BARCA B, fire activity was low throughout the Amazon region due to heavy precipitation, while during BARCA A, intense fire activity occurred on the northern coast of Brazil and scattered fires were present throughout the southeastern Amazon.

Andreae et al. (2012) summarized the BARCA campaign, meteorological background, carbon monoxide and aerosol observations and CO results from several regional transport and chemistry models. These included the CCATT-BRAMS and WRF-Chem simulations analyzed in greater detail in this paper. Meteorological analysis showed that during BARCA A, when the Inter-Tropical Convergence Zone (ITCZ) was to the north of the Amazon Basin, inflow to the Amazon was primarily from the Southern Hemisphere. During BARCA B, the ITCZ extended to 20° S and air at low levels was of Northern Hemisphere origin, including some smoke from West African fires. On the other hand, the mid-tropospheric air was of mixed origin.

The highest CO levels were observed on the flights on 25-27 November in the southeastern Amazon, influenced by regional biomass burning, since maximum values were observed from 1-3 km. These are typical of injection heights of smoke plumes from savanna fires (Freitas et al., 2007). The excess CO from biomass burning was between about 30 and 200 ppb, increasing from north to south across the Basin. According to analysis of tracer simulations, during BARCA A biomass burning contributed on average about 56 ppb (31%) to the total CO of around 180 ppb, while the background was 110 ppb (61%). Biomass burning influence was indicated by CO mixing ratios up to 300 ppb, Condensation Nuclei (CN) approaching 10000 cm^{-3}, and a low CN to CO ratio ($\Delta CN/\Delta CO$) signifying aged smoke. This influence was highest in the southern Amazon from 1-3 km. Manaus back trajectories at 500 and 4000 m came from eastern Amazon fires rather than the intense African fires occurring at the same time. During BARCA B, little biomass burning influence was observed. CN counts were 300-500 cm^{-3} and a CO enhancement of ~10 ppb above the mixing ratios in air entering the Basin from the Atlantic was seen. Small boundary layer enhancements were attributed to a source from the oxidation of biogenic VOCs (Andreae et al., 2012).

Andreae et al. (2012) also showed simulated vertical CO profiles from CCATT-BRAMS and WRF-Chem simulations, as well as the Stochastic Time Inverted Lagrangian Transport (STILT) model with two different meteorological field inputs and the WRF Greenhouse Gas Module (WRF-GHG). The simulated CO profiles matched mean observed values, but were overly vertical (too low near the surface and too high above 3 km). This suggested that the models had too much convective transport or vertical mixing from the PBL schemes. However, the probability densities were consistent with observations in the boundary layer, indicating that horizontal dispersion was reasonable. Beck et al. (2013) evaluated different CH_4 wetland emissions schemes and maps using WRF-GHG. They found the best agreement with BARCA CH_4 data for days where convective transport, as evaluated by comparison of upstream TRMM and WRF precipitation amounts, was well represented in the model. This indicates that proper representation of convective transport in models is essential for prediction of vertical distributions of pollutants in the Amazon Basin.

It is interesting to compare BARCA data to observations from the NASA Amazon Boundary Layer Experiments ABLE campaigns (ABLE-2A and -2B), which took place during the dry season of 1985 and wet-to-dry transition of 1987. During the dry season (July-August 1985), the Amazon Boundary Layer Experiment (ABLE-2A) integrated aircraft, ground-based and satellite observations to study the processes affecting the chemical composition in mixed layer over Amazonia (Harriss et al., 1988). Jacob and Wofsy (1988) used a photochemical model of the Amazonian boundary layer to study the diurnal cycle of isoprene, NO_y and O_3 during ABLE-2A. They found that photochemical production spurred by NO emissions from soils increased daytime O_3 to about 20 ppb. However, at night, dry deposition to the forest caused O_3 to drop below 5 ppb. Model results were consistent with the NO values of 25-60 ppt observed in the lower boundary layer over central Amazonia (Torres and Buchan, 1988). Isoprene emissions were found to have little effect on O_3 levels, as the oxidation of CO would produce sufficient HO_x to generate 20 ppb of O_3. However, O_3 production in the model was highly sensitive to NO_x emissions, and downward transport from the free troposphere became the dominant source of O_3 in the PBL when NO emissions were decreased below the average value of 44 ± 14 μg N m^{-2} h^{-1} NO measured by Kaplan et al. (1988). Lidar observations during ABLE-2A showed highly variable O_3 levels, with some small regions with up to 30-40 ppb, attributed to variable NO flux from the canopy (Browell et al., 1988). ABLE-2B was conducted during the wet-to-dry transition season (April-May 1987) (Harriss et al., 1990). Periodic inputs from the Northern Hemisphere were found to be a pollution source over Amazonia, and dry deposition in the region provided a significant sink in the global O_3 budget. As part of ABLE-2, near-continuous O_3 surface measurements (1.5 m above the soil surface) showed daytime maximums of 3.7 ppb inside a forest and 5.7 ppb in a clearing (typical standard deviations of 0.3 ppb). Additionally, tower measurements at the clearing site showed higher O_3 values of 6.7 ppb at 7 m above the soil surface and 6.9 ppb at 15 m above the soil surface (Kirchhoff et al., 1990). Furthermore, 20 ozonesondes launched in the clearing showed typical mixing ratios of 40 ppb from 500-300 hPa, with values about 10 ppb lower in the wet than dry season.

Andreae et al. (2012) showed that CO mixing ratios were about 10 ppb higher during ABLE-2B than in BARCA B everywhere except the southern region, reflecting the global trend towards decreasing CO emissions since the 1980s, particularly in the Northern Hemisphere. The CO comparison also showed a similar enhancement of 10–20 ppb in the lowest 1 km above the surface, attributed to diffuse biogenic sources, and also indicated that the much higher enhancements during the dry season in BARCA A must be due to anthropogenic or biomass burning inputs. The O_3 comparison is expected to yield information in long-term trends in O_3 production in the Amazon Basin, as well as the relative importance of biogenic, urban and fire sources.

3 Data and Methods

3.1 BARCA aircraft measurements

During the BARCA campaign, in-situ measurements of O_3 were conducted aboard the EMB 110 Bandeirante INPE aircraft using a dual-cell, UV Photometric analyzer (Ozone Analyzer, Model 49i, Thermo Fisher Scientific, United States). During BARCA A, 1 minute averages of the original 1 second data were taken, while during BARCA B 1 second data were stored. The detection limit for both campaigns was 1 ppb. The intake for O_3 was forward-facing, located 185 mm from the fuselage on the lower fuselage in front of the propellers to minimize effects of turbulence. The inlet lines consisted of stainless steel tubes with a bend radius of 100 mm and an inner diameter of 11.5 mm. The sample air was not heated or dried before measurement, so reported values are molar mixing rations, nmol mol^{-1}, abbreviated 'ppb', with respect to ambient humid air (Andreae et al., 2012).

3.2 Model description and simulation setup

Simulations of BARCA A and B were conducted with the Chemistry Coupled Aerosol-Tracer Transport model to the Brazilian developments on the Regional Atmospheric Modeling System (CCATT-BRAMS; Longo et al., 2013; Freitas et al., 2009) and Weather Research and Forecasting with Chemistry (WRF-Chem; Grell et al., 2005) coupled chemistry and meteorology models. The model physics and chemistry options that were used are listed in Table 1. Both models used a two-way nested grid configuration, with a 140 km grid covering Africa and South America (southwest corner: 60°S, 100°W, northeast corner: 20°N, 50°W), to encompass the cross-Atlantic transport of biomass burning emissions from Africa, and a 35 km resolution grid covering most of South America (southwest corner: 35°S 85°W, northeast corner: 15°N, 30°W), as depicted in Fig. 3.

The simulations were initialized on 1 October 2008 00:00 UTC and 1 April 2009 00:00 UTC for BARCA A and B, respectively. Boundary conditions and analysis nudging on the outer domain were given by the NCEP GFS analysis (http://rda.ucar.edu/datasets/ds083.2/) with a 6 hourly time resolution and 1° × 1° spatial resolution. Chemistry initial and boundary conditions were provided by 6 hourly analyses from the Model of Atmospheric Chemistry at Large Scale (Modélisation de la Chimie Atmosphérique Grande Echelle, MOCAGE) global model (Peuch et al., 1999) with a T42 (~ 2.8°) spatial resolution. Sea surface temperature was provided by the NOAA Optimum Interpolation (OI) Sea Surface Temperature (SST) V2 (available at http://www.esrl.noaa.gov/psd/data/gridded/data.noaa.oisst.v2.html) with 1° × 1° spatial resolution. Soil moisture was initialized with the TRMM-based soil moisture operational product (GPNR) developed by Gevaerd and Freitas (2006).

The PBL parameterization in CCATT-BRAMS is based on Mellor and Yamada (1982), while in WRF-Chem the Mellor-Yamada-Janjic (MYJ; Janjić, 1994) scheme was used. In CCATT-BRAMS, shallow and deep convection are parameterized based on the mass-flux approach of Grell and Dévényi (2002). CCATT-BRAMS also uses the Turbulent Kinetic Energy (TKE) from the Planetary Boundary Layer (PBL) scheme to determine if convection will be triggered within a grid cell. In WRF-Chem the Grell 3D (G3) scheme was used, which includes shallow convection and subsidence spreading of convective outflow into neighboring grid cells. The Noah land surface model (Koren et al., 1999) was used in WRF-Chem and the Land Ecosystem–Atmosphere Feedback model v.2 (LEAF-2; Walko et al., 2000) was utilized in CCATT-BRAMS. Land use was provided by the United States Geological Survey (USGS) global 1 km vegetation dataset, updated with a land cover map for the Brazilian Legal Amazon Region for use in meteorological models (PROVEG) (Sestini et al., 2003). PROVEG is based on the Thematic Mapper (TM) Landsat images with spatial resolution of 90 m × 90 m from the year 2000 and deforestation data from the Amazon Deforestation Monitoring Program (PRODES) for the year 1997. For WRF-Chem, albedo and greenness fraction were calculated offline using the updated vegetation dataset, Moderate Resolution Imaging Spectroradiometer (MODIS) Normalized Difference Vegetation Index (NDVI) data from the years 2001-2002 and vegetation parameters from the LEAF-2 land surface model as implemented in CCATT-BRAMS.

Emissions were generated with PREP-CHEM-SRC (Freitas et al., 2011) Version 1.2. Fire emissions were estimated from GOES, AVHRR and MODIS fire count data using the Brazilian Biomass Burning Emission Model (3BEM; Longo et al., 2009). Anthropogenic emissions were estimated from the RETRO, GOCART and EDGAR v4.0 global databases updated with South American inventories (Alonso et al., 2010). Emissions are obtained from RETRO if available for that species (CO, NO_x, chlorinated hydrocarbons, acids, esters, alcohols, ethers, benzene, ketones, methanal, other alkanals, other aromatics, C_2H_2, C_2H_4, C_2H_6, C_3H_6, C_3H_8, C_4H_{10}, C_5H_{12}, C_6H_{14} plus higher alkanes, other VOCs, toluene, trimethylbenzenes, xylene), then from EDGAR v4.0 (NMVOC, SO_4, CO_2, SF_6, N_2O), otherwise from GOCART (BC, OC, SO_2, DMS), in order to use the most consistent emissions inventory possible. Biogenic emissions were provided by a monthly climatology for the year 2000 produced with the Model of Emissions of Gases and Aerosols from Nature (MEGAN; Guenther et al., 2006). The MEGAN 2000 climatology includes numerous biogenic species (acetaldehyde, formaldehyde, other ketones, acetone, isoprene, propane, methane, propene, ethane, methanol, sesquiterpenes, ethene, monoterpenes and toluene), but not soil NO emissions. In WRF-Chem, the same

Gaussian diurnal cycle with peak at 15:00 UTC (11:00 LT) is applied to both anthropogenic and biogenic emissions, while in CCATT-BRAMS the diurnal cycle of biogenic emissions follows the solar radiation cycle. In both models, the biomass burning daily cycle peaks at 18:00 UTC (15:00 LT).

In both CCATT-BRAMS and WRF-Chem, the Regional Atmospheric Chemistry Mechanism (RACM) was used (Stockwell et al., 1997). In WRF-Chem, the Goddard Chemistry Aerosol Radiation and Transport (GOCART; Chin et al., 2002) aerosol scheme was used with aerosol direct radiative effects. CCATT-BRAMS has a smoke aerosol scheme with intensive optical properties (extinction efficiency, single scattering albedo and asymmetry parameter) calculated in an offline Mie code based on observations of climatological size distribution and complex refractive index from AERONET sites in the southern Amazon (Rosario et al., 2011, 2013).

CCATT-BRAMS includes scavenging of soluble species in the convective scheme following Berge (1993), as described in Freitas et al. (2005), where the wet removal rates are a function of the precipitation rate, liquid water content and precipitable water. In the cloud microphysics scheme the wet deposition follows Barth et al. (2001), whereby low solubility species partition into the liquid phase according to Henry's Law and high solubility species by diffusion-limited mass transfer. In WRF-Chem, at the convective-parameterizing scale, a constant fraction of gas and aerosol species in convective updrafts are removed (complete removal for sulfur dioxide – SO_2, sulfate – H_2SO_4, ammonium – NH_3, nitric acid – HNO_3 and sea salt; no removal for hydrophobic organic (OC) and black carbon (BC) and dimethyl sulfide (DMS); and 50% removal for all other aerosol species). On the other hand, no wet scavenging is included for cloud water and precipitation resolved by the microphysics scheme, because this option is not currently available in WRF-Chem for the RACM chemical mechanism. O_3 production in the upper troposphere is affected by the net convective transport of soluble HO_x precursors (including hydrogen peroxide (H_2O_2), methyl hydroperoxide (CH_3OOH) and formaldehyde (CH_2O)). However, uncertainties remain about the scavenging efficiencies of soluble species by deep convective storms. Simulations of an idealized thunderstorm by several cloud-resolving models yielded varying results for CH_2O, H_2O_2 and HNO_3 in convective outflow due to differing microphysics and assumptions about retention of chemical species during cloud drop freezing (Barth et al., 2007).

The CCATT-BRAMS simulations employ a lightning NO_x parameterization based on convective cloud top height (Stockwell et al., 1999). In WRF-Chem, lightning production of NO_x was not included, because these parameterizations have not yet been evaluated for the Amazon region. In the tropics, over continents, lightning production is comparable to other sources of NO_x, including biomass burning and soil release, and it is the primary source over oceans (Bond et al. 2002). Since lightning NO_x production peaks in the upper troposphere, it could be an important contributor to ozone production. The roles of wet deposition and lightning NO_x production will be more closely examined in future modeling studies of tropospheric chemistry in the Amazon.

For model results evaluation, the mean vertical O_3 profiles for observations, CCATT-BRAMS and WRF-Chem were calculated for the regions to the west, north, south, east, and around Manaus. Horizontal flight legs were excluded from analysis to eliminate the influence of plumes in the boundary layer. As the model output has a much coarser spatial and temporal resolution than the aircraft measurements, the model value is interpolated to the observation time and location. To calculate the mean simulated profiles, the four grid points closest in latitude and longitude to each observation were determined at the two model hours that bracket the observations. At each of these grid points and hours, vertical profiles were extracted from the model output and then linearly interpolated to the observed GPS height. The four points from each time were averaged, weighting by the inverse distance to the observed longitude and latitude. Finally, the prior and posterior hour values were averaged with appropriate weights. Thus, 16 model points were used with spatial and temporal weights to obtain each model value for comparison to observations. The observed and model time series were then separated into five regions to the west, north, east, and south of Manaus, and in the region of Manaus itself. The mean value and standard deviation were calculated for each region and 500 m vertical bin. To facilitate comparison of other models with the data presented in Fig. 2, mean profiles from the large regions corresponding to clean (west, north and around Manaus regions) and polluted (east and south regions) regions during BARCA A and all regions during BARCA B are presented in Fig. 16. From the models, all horizontal grid points falling within the corresponding region's longitude and latitude bounds for each flight day (Table 6) and the closest model output times (12:00-18:00 UTC / 8:00-14:00 LT) were averaged into 500 m vertical bins.

3.3 Meteorological and satellite and ground-based O_3 data

Monthly mean precipitation over the Amazon region was obtained from the 3B43 Tropical Rainfall Monitoring Mission (TRMM) and Other Data Precipitation Product at a spatial resolution of 0.25° × 0.25° (obtained from http://trmm.gsfc.nasa.gov/) (Kummerow et al., 1998; Kawanishi et al., 2000). TRMM 3B43 is derived from retrievals of 3-hourly precipitation amount from the Precipitation Radar (PR), TRMM Microwave Imager (TMI), and Visible and Infrared Scanner (VIRS) aboard the TRMM satellite, merged with rain gauge data from Climate Anomaly Monitoring System (CAMS) and the Global Precipitation Climatology Project (GPCP). Satellite estimates of precipitation are used for model evaluation due to their more complete spatial and temporal coverage compared to rain gauge data. Buarque et al. (2011) found that mean annual rainfall from Brazilian rain gauge and TRMM 3B42 3-hourly data at 488 sites in the Amazon Basin for the years 2003-2005 agreed within 5%. Other characteristics of the rainfall distribution, such as the number of days with rainfall, differed more substantially. Mean precipitation during the dry-to-wet (Nov. 2008) and wet-to-dry (May 2009) transition seasons was calculated for the TRMM 3B43 data and the CCATT-BRAMS and WRF-Chem models for three regions: the Amazon (15°S – 10°N, 50°W – 80°W), northeast Brazil (15°S – 0°N, 35°W – 50°W), and southeast South America (15°S – 35°S, 35°W – 65°W). The values are listed in Table 2. The mean precipitation on the 35 km resolution domain for the two months is shown in Fig. 4, as well as the delineations of the subregion boxes.

Surface downward shortwave radiation (Level 1.5) obtained with a Kipp and Zonen CM-21 pyranometer (305-2800 nm) were obtained from the Solar Radiation Network (SolRad-Net) site at Manaus (2.56°S, 60.04°W, 93 m a.s.l.) (http://aeronet.gsfc.nasa.gov/cgi-bin/bamgomas_interactive) (Fig. 5).

Mean daily cycles of fluxes of sensible and latent heat and radiation were obtained from flux tower measurements for the wet (February - March 1999, January - March 2000) and dry (July - September 1999-2000) seasons at forest (Rebio Jarú, 10.08°S, 61.93°W, 145 m a.s.l.) and pasture (Fazenda Nossa Senhora, 10.75°S, 62.37°W, 293 m a.s.l) tower sites (von Randow et al., 2004) (Figs. 6-7).

Surface meteorological station data was obtained for the BARCA region for October - November 2008 and April - May 2009 from 52 SYNOP (INMET) and 26 METAR (airport) stations, the locations of which are depicted in Fig. 10. The models were also evaluated against TRMM 3B42 3-hourly precipitation rates at the 78 surface station locations in the Amazon. Mean observations and values of Root Mean Squared Error (RMSE) and bias for the CCATT-BRAMS and WRF-Chem simulations are shown in Table 3.

Meteorological soundings from the Manaus airport (3.15°S, 59.98°W) were conducted at 00:00 UTC (12 in October-November 2008, 60 in April-May 2009) and 12:00 UTC (49 in October - November 2008, 60 in April - May 2009). During BARCA A, 13 additional soundings were conducted at 18:00 UTC from 18 November – 1 December 2008 (Figs. 8-9).

Fisch et al. (2004) found that in the dry season (14-25 August, 1994), higher sensible heat fluxes over pasture increase the maximum height at 21:00 UTC (17:00 LT) of the Convective Boundary Layer (CBL) from around 1100 m for forest (Rebio Jarú) to 1650 m over pasture (FNS). On the other hand, during the wet season (January-February 1999) the height of the CBL was similar for both land types, around 1000 m. The simulated height of the PBL at 21:00 UTC above the forest and pasture sites (Table 4) was analyzed from model output using two different methods: *TKE*, the first level above the surface where the Turbulent Kinetic Energy (TKE) from the PBL schemes dropped below 0.01 $m^2 s^{-1}$ and *Theta*, the first level above the surface where theta exceeded theta of the level below by 0.6 K. In addition, *WRF MYNN* is the diagnostic from the WRF PBL scheme which takes into account TKE as well as stability.

In addition to the in-situ O_3 data, the model results were compared with OMI/MLS monthly mean tropospheric ozone mixing ratios and total column ozone (http://acd-ext.gsfc.nasa.gov/Data_services/cloud_slice/#pub) (Ziemke et al., 2006) (Fig. 20-21). In this product, the tropospheric values are estimated by subtracting the stratospheric contribution from total column measurements. A cloud-slicing method is used to detect O_3 inside optically thick clouds. This method is able to detect elevated O_3 levels of around 50 ppb in the upper parts of convective clouds over South America and Africa, comparable to background cloud-free levels in the tropics (Ziemke et al., 2009). In this study, the model total tropospheric O_3 column and mean tropospheric O_3 mixing ratio were calculated by summing O_3 mixing ratios, weighted by the model level air density, from the first model level to the level below the tropopause. The tropopause level was determined by the World Meteorological Organization (WMO) definition of a temperature lapse rate less than 2 K km^{-1} (Logan, 1999).

The models were also compared with soundings measuring O_3, temperature, and relative humidity conducted at sites in Paramaribo, Surinam (5.8°N, 55.2W) and Natal, Brazil (5.4°S, 5.4°W) during the BARCA periods as part of the Southern Hemisphere ADditional OZonesondes (SHADOZ) network (http://croc.gsfc.nasa.gov/shadoz/) (Thompson et al., 2003a, b, 2007) (Fig. 22).

4 Results and discussion

4.1 BARCA O_3 Observations

The vertical distributions of O_3 measured by the aircraft during BARCA A and B are depicted in Fig. 2. Observations during the dry-to-wet transition (BARCA A) are plotted separately for clean (west, north and around Manaus regions) and fire-influenced polluted (east and south regions) conditions. The longitude and latitude bounds and flight dates included in each geographic region from BARCA A and BARCA B are listed in Table 6. The O_3 distributions are similar during BARCA A in the clean regions and BARCA B, with median values ranging from 10-25 ppb. However, there is more variability, as measured by the difference between the 25th and 75th percentiles, in the BARCA A data. This may be due to downward mixing of O_3 transported long-range from fires in Africa or recirculated from the polluted southeast Brazil region. In the fire-influenced regions during BARCA A, medians range from 25-45 ppb, peaking at a typical plume injection height for savanna fires of 2-3 km. The highest variability is seen in polluted conditions during BARCA A, particularly at 2-3 km, indicating the influence of small-scale fire plumes. This variability of O_3 in the PBL presents a challenge to the regional models, since the effects of small-scale processes such as plume rise and convection are parameterized and averaged across the grid cell.

4.2 Observed and Simulated Meteorology

Tropospheric O_3 distributions are driven by both chemical processes, including chemistry and emissions of O_3 precursors, and meteorological ones, such as solar radiation, tracer transport and removal. During the dry-to-wet transition season, increased actinic fluxes stimulate the production of OH radicals from O_3 photolysis that can lead to net O_3 production (Seinfeld and Pandis, 2006). In November 2008, a band of increased precipitation extended in TRMM 3B43 observations from the northwest Amazon to southeast Brazil but the northern Amazon between Manaus and Belém was relatively dry (Fig. 4a). On the other hand, in the wet-to-dry transition season, lower levels of O_3 are largely associated with increased presence of convective clouds and precipitation. Decreased surface temperatures and incident solar radiation due to cloudiness suppress emissions of biogenic VOCs such as isoprene (Fall and Wildermuth, 1998). In addition, higher surface humidity and precipitation decrease the occurrence of fires (Morton et al., 2013; Chen et al., 2013) that emit NO_x and VOCs (Freitas et al., 2007). O_3 precursors are further decreased by wet removal within the storms (Barth et al., 2007a). In May 2009, increased precipitation as observed by TRMM 3B43 extended from the western Amazon to the northeast coast of Brazil (Fig. 4b). In radiosoundings at Manaus, a more pronounced decrease in dew point temperature from 0:00 UTC to 12:00 UTC is observed in May 2009 (Fig. 9) than Nov. 2008 (Fig. 8) in upper levels (300-400 hPa), likely due to more precipitation.

Land cover also impacts surface heat and moisture exchange and can thus affect convective triggering. In both transition seasons, surface sensible heat fluxes are higher and latent heat fluxes are lower at the pasture compared to forest sites (Figs. 6a-b and 7a-b). However, incident solar radiation and thereby peak sensible heat flux (Fig. 7) are lower in the wet-to-dry than dry-to-wet transitions (Fig. 6) for both forest and pasture sites.

Now we summarize the key findings of the model-data meteorological comparison and their implications for the chemistry simulations. The models capture the seasonal spatial distribution of precipitation over northern South America signs of NE-SE differences are correctly modeled by both models during both seasons, i.e., the NE is drier than the SE during November, and vice-versa during May. For the Amazon, CCATT-BRAMS slightly underestimates the precipitation rates in both seasons, but the rate in WRF-Chem is about twice that of TRMM 3B43 (Table 2). This may lead to errors in the strength and vertical distribution of convective transport and the amount of convective wet removal.

Peak surface shortwave radiation during the dry-to-wet transition at Manaus is within the error bars of the observations for both models (Fig. 5). However, for the southern Amazon forest and pasture sites peak shortwave may be overestimated (underestimated) by 50-100 W m^{-2} by CCATT-BRAMS (WRF-Chem) (Figs. 6-7), suggesting that there is insufficient (excessive) cloudiness in the models. This will increase (decrease) surface temperature and evaporation, and therefore increase (decrease) O_3 production from photolysis.

In the dry-to-wet transition season (Fig. 7), the observed Bowen ratio (sensible/latent heat flux) is lower at the forest site than the pasture site (0.23-0.38 vs. 0.8). However, in WRF-Chem, the Bowen ratio at 13:00 LT shows a smaller contrast between the forest and pasture sites (0.40 vs. 0.51), due to underestimated sensible heat flux at the pasture site. In the wet-to-dry transition season (Fig. 8), the observed Bowen ratio is lower at both forest and pasture sites for this season (0.18-0.39 vs. 0.33-0.59). On the other hand, in WRF-Chem, latent and sensible heat flux and thus the Bowen ratio are nearly constant at the forest and pasture sites (0.39 vs. 0.38). This indicates that the Noah land surface model is not properly representing the impact of conversion of forest to pasture and the resulting increase in sensible heat flux.

At the surface stations (Table 3), both models overestimate precipitation on average. Dew point temperature is underestimated by 1-2 K and temperature is underestimated in all cases by 0.1 - 2.4 K except by CCATT-BRAMS during BARCA A, which overestimated temperature by about 1 K. All of these biases will decrease photochemical O_3 production at the surface. The models generally show good agreement with soundings at Manaus, but excess moisture (positive dewpoint bias of 10 K) in CCATT-BRAMS above 500 hPa may lead to increased O_3 production at mid-levels.

Next we compare the CBL heights for wet and dry seasons reported by Fisch et al. (2004) with the simulated PBL heights in the dry-to-wet and wet-to-dry transitions (Table 4). The models represent the pattern of lower PBL heights in the wet-to-dry than dry-to-wet transitions, and similar PBL heights at the forest and pasture sites. However, for the dry-to-wet transition, the PBL heights are indistinguishable between forest and pasture sites for both models, and generally closer to the observed forest (1.1 km) than pasture (1.65 km) values. Additionally, for the wet-to-dry transition, the mean PBL height for all models and diagnostics except *Theta* for CCATT-BRAMS are lower than observed (1 km). Overall the models underestimate the PBL depth, which may contribute to an overestimate of O_3 near the ground. Despite these limitations, the models are able to capture the meteorological contrast between the dry-to-wet and wet-to-dry transition seasons.

4.3 Observed and Simulated Chemistry

4.3.1 Mean O_3 Profiles

An example of observed and simulated O_3 during the flight legs between Manaus and Belém in BARCA A and B is shown in Fig. 17. While the models capture the pattern of increasing O_3 values with height, the models underestimate elevated O_3 values from 2.5-4.5 km, and overestimate low values near the surface (1-1.5 km). The models also do not reproduce the variability in the high values, likely due to the aircraft intersection of biomass burning plumes. This is expected given the coarse horizontal grid resolution. Thus, mean profiles are analyzed in order to study differences among the regions and seasons and to assess the models' abilities to capture the impacts of such small-scale processes on regional O_3 distributions.

The mean vertical O_3 profiles for observations, CCATT-BRAMS and WRF-Chem for the regions to the west, north, south, east and around Manaus are shown for BARCA A and B in Figs. 12 and 14, respectively, and NO profiles corresponding to the aircraft tracks are depicted in Figs. 13 and 15, respectively. Mean profiles from longitudinal surveys over Amazonia of O_3 during ABLE-2A (Browell et al., 1988) and ABLE-2B (Harriss et al., 1990) and NO during ABLE-2A (Torres and Buchan, 1988) are included for comparison. In BARCA B, O_3 values were at or near background values in all regions, ranging from 8 - 15 ppb at the surface to 2 - 15 ppb at 4 - 4.5 km, and the models are generally within 5 - 10 ppb of the observations. During BARCA A, while the W region still had low O_3 values (5 ppb at the surface to 20 ppb at 4 - 4.5 km), the N, S and M regions ranged from 15 - 20 ppb at the surface to 30 - 35 ppb at 4 - 4.5 km, and the E region presented the most elevated values, from 25 - 55 ppb. ABLE-2A O_3 profiles are similar in all regions, ranging from 15 - 20 ppb near the surface to 30 - 40 ppb from 4 - 6 km, so that the BARCA values are higher in the fire-influenced east and south regions, lower in the north and west regions, and very similar around Manaus. The profiles from ABLE-2B are within one standard deviation of the BARCA B measurements, except for the north region, where they are lower (5-15 ppb). These results suggest an increasing influence of fire emissions to the east and south of Manaus, but that O_3 in clean regions has not changed much.

A similar model behavior is seen in the broad regional mean profiles (Fig. 16). All simulations over-estimate O_3 throughout the PBL and lower troposphere during clean conditions in BARCA A, but under-estimate O_3 in polluted conditions. This is especially true from 2-4 km where biomass burning plumes detrain O_3 precursors. During BARCA B all simulations show good agreement.

In order to understand the possible sources of model error, we now individually examine the contributions of different chemical sources and sinks, including surface emissions and deposition, boundary inflow and chemistry within the PBL.

4.3.2 Emissions

The relative sensitivities of O_3 production to NO_x or BVOC emissions depend upon the relative amounts of VOCs and NO_x present. Under clean conditions with a high VOC:NO_x ratio, O_3 production is NO_x sensitive, whereby increases in NO_x will lead to increases in O_3 while increased VOCs will have little impact. On the other hand, in polluted areas with a high NO_x:VOC ratio, the system is VOC-sensitive, that is, increased VOCs contribute to O_3 production but an increase in NO_x actually depletes O_3. Emissions of BVOCs can increase O_3 production by the following mechanism. Oxidation of BVOCs can lead to formation of HO_2 and $RO_2\bullet$, which react with NO to form NO_2. NO_2 in turn photolyzes to form $O(^3P)$, which reacts with O_2 to form O_3 (National Research Council, 1991). We expect the polluted east/south regions during BARCA A to be VOC-sensitive and the clean west, north and around Manaus regions during BARCA A and all regions in BARCA B to be NO_x-sensitive. Kuhn et al. (2010) determined via aircraft transects in the Manaus urban plume that most of the VOC reactivity was provided by isoprene emissions from the surrounding rainforest, and NO_x emissions suppressed O_3 production close to urban sources, but stimulated it downwind.

For BARCA, the simulated mean monthly emission rates for two O_3 precursors, NO_x (anthropogenic and biomass burning) and isoprene (biogenic) are shown in Fig. 17. In Nov. 2008, elevated NO_x emission rates of up to 5 x 10^{-5} kg m^{-2} day^{-1} are seen from an area of intense biomass burning in the northeast Amazon, as well as from more scattered fires in the southeast Amazon. These are both regions that were overflown by the aircraft (Fig. 1). In May 2009, the Amazon region is largely free of fire. Because biogenic NO emissions (e.g., from soil) were not included in the MEGAN climatology used in this study, background NO emissions (in absence of fire) are likely too low.

Typical model anthropogenic NO_x emissions values over the Amazon, primarily from biofuel sources, were 0.008-13 μg N m^{-2} hr^{-1} N. This NO_x emissions included in the modles were less than one third of the mean values of 44 ± 14 μg N m^{-2} h^{-1} NO measured by Kaplan et al. (1988) during ABLE-2A. This is considered a threshold value for NO_x-driven O_3 production to be the dominant O_3 source in the PBL. The model emissions were also much lower than the mean emissions from forest of 35.8 μg N m^{-2} h^{-1} NO measured in the 1998 dry season (Garcia-Montiel et al., 2003). Wetting the forest soil resulted in small pulses of NO and therefore the mean emissions are expected to be higher in the wet season than dry season.

Isoprene emissions are highest in the western and southern Amazon, reaching 15 x 10^{-5} kg m^{-2} d^{-1} in November 2008 and 5-10 x 10^{-5} kg m^{-2} d^{-1} in the aircraft sampling region. Due to decreased surface temperature and incident solar radiation in the rainy season, isoprene emissions in the Amazon Basin are much lower during BARCA B, 3-5 x 10^{-5} kg m^{-2} d^{-1}. The MEGAN emissions are consistent with isoprene emission measurements above the Amazonian canopy: a normalized flux of 5.76 x 10^{-5} kg m^{-2} d^{-1} in July 2000 at the end of the rainy season (Rinne et al., 2002) and an average noontime flux of 18.7 ± 5.5 x 10^{-5} kg m^{-2} d^{-1} in September 2004 during the dry season (Karl et al., 2007).

4.3.3 Deposition

Figures 18 and 19 show the average O_3 dry deposition flux and median daytime deposition velocity, respectively, as simulated on the 35 km resolution domain by the CCATT-BRAMS and WRF-Chem models for November 2008 and May 2009. In the Amazon Basin, O_3 deposition fluxes are higher in the dry-to-wet transition season, with values reaching 3.5 nmol m^{-2} s^{-1} for CCATT-BRAMS and 6 nmol m^{-2} s^{-1} for WRF-Chem in the northeast Amazon, near the region of concentrated biomass burning. These values are also seen along the northern Andes and Southeast Brazil, due to recirculation of O_3–rich air. In the wet-to-dry transition season, O_3 deposition is at a minimum in the western Amazon, with values of 0.5-1 nmol m^{-2} s^{-1} for CCATT-BRAMS and 2 nmol m^{-2} s^{-1} for WRF-Chem. For both models, deposition velocities are higher over the rainforest than in the savanna to the east or south of the Amazon Basin, and higher in the wet-to-dry transition than in the dry-to-wet transition. These patterns are also seen in the tower observations in Table 5.

O_3 surface fluxes and dry deposition velocities predicted by the models were compared with observations from several field campaigns (Table 5). These include during the dry (May 1999) and wet (September–October 1999) seasons at Reserva Biológica Jarú (RBJ, forest) and Fazenda Nossa Senhora (FNS, pasture) from LBA-EUSTACH (Rummel et al., 2009; Kirkman et al., 2002) and during the wet season at Reserva Ducke (RD, forest tower near Manaus, 2.95°S, 59.95°W°) from ABLE 2B (April-May

1987) (Fan et al., 1990) and at FNS from LBA-TRMM (January - February 1999 (Sigler et al., 2002). For the observations, the means of the hourly (WRF-Chem) and 3-hourly (CCATT-BRAMS) O_3 dry deposition fluxes (nmol m^{-2} s^{-1}) and the medians of the daytime (11:00 – 21:00 UTC) hourly mean deposition velocities (cm s^{-1}) are shown. The values were extracted from the grid points closest to the tower locations. In the observations, O_3 fluxes are larger in the dry season, due to higher O_3 mixing ratios. However, deposition velocities are higher in the wet season, and O_3 deposition to the Amazon forest constitutes a globally significant O_3 sink (Rummel et al., 2009). Both models capture these patterns, but the models underestimate the deposition velocities by 15-75%, which may be partially responsible for the low O_3 fluxes at the Jarú forest site in both seasons and the pasture site in the dry season.

4.3.4 Boundary Conditions

The mean tropospheric and total tropospheric column O_3 from OMI/MLS, CCATT-BRAMS and WRF-Chem for November 2008 and May 2009 are shown in Figs. 20 and 21, respectively. The models significantly underestimate the total columns from satellite and middle altitudes from BARCA. For both BARCA A and B, the models represent the pattern of lower O_3 over the Amazon and higher values over northeast Brazil (BARCA A only) and at 30°S, although the values are strongly underestimated. In November 2008, OMI/MLS mean tropospheric O_3 concentrations show an inflow of elevated O_3 (mean ca. 55 ppb, total 40-45 DU) on the northeast Brazilian coast due to cross-Atlantic transport from biomass burning in southern and sub-Saharan Africa. Additionally, a band of elevated O_3 (mean 55-60 ppb, total 35-40 DU) passes over the South American continent at around 30°S, also from cross-Atlantic transport. During this month, Northern Hemisphere O_3 levels to the north of South America are relatively low (mean 35-40 ppb, total 25-30 DU). On the other hand, the tropospheric ozone distribution in May 2009 (Fig. 16) is characterized by a band of low ozone extending over the Amazon Basin and northeast Brazil between 10°S and 10°N (mean 25-35 ppb, total 20-25 DU). In addition, slightly elevated values at around 30°S, primarily over the oceans (40-55 ppb, 30-35 DU) and higher ozone in the Northern Hemisphere (mean 50-55 ppb, total 35-40 DU north of 10°N). Both models capture the overall distribution (inflow in NE Brazil in Nov. 2008, lower values over the Amazon Basin, elevated at 30°S) but values are underestimated relative to OMI/MLS. In general the models overestimate O_3 in the PBL compared to aircraft measurements, but underestimate the total column values relative to the OMI/MLS satellite product. This suggests that the total column values in Amazonia are dominated by global pollution from Africa, rather than local O_3 production from biomass burning. A typical OMI averaging kernel (cloud-free ocean conditions) shows maximum sensitivity from 594-416 hPa (Zhang et al., 2010). Therefore, OMI may not be detecting O_3 in the PBL from local sources, but rather primarily seeing global pollution from Africa.

Above the boundary layer, from 3-4 km a.g.l., chemical inflow at the eastern boundary of South America may contribute to O_3 elevated above background. In order to evaluate the model representation of this inflow, vertical profiles from SHADOZ soundings on the northeast coast of South America during the BARCA A and B periods were compared with CCATT-BRAMS and WRF-Chem (Fig. 22). In addition, 120 h back trajectories from the sounding locations at heights of 1500 m, 6000 and 9000 m above ground level (gal) were calculated with the HYSPLIT model (http://ready.arl.noaa.gov/hypub-bin/trajtype.pl?runtype=archive) using meteorological data from the NCEP/NCAR global reanalysis. Inflow at Paramaribo originated either in the Caribbean or the tropical Atlantic, while at Natal, air parcels came from anti-cyclonic recirculation from southeastern Brazil or the tropical Atlantic. Both models generally represent the SHADOZ O_3 profiles up to 600 hPa, but do not capture layers of elevated O_3 above 500 hPa. These are likely to be either from pollution recirculated from southeast Brazil or possibly from African biomass burning. The models also do not reproduce thinner layers of high O_3 below 600 hPa. For example, at Natal on 7 November 2008 (Fig. 22c, air of African origin at ~850 hPa and ~470 hPa) and 19 November 2008 (Fig. 22d, air from the central African coast at ~850 hPa and recirculation from southeastern Brazil at ~470 hPa and ~310 hPa) and at Paramaribo on 11 May 2009 (Fig. 22f, air of tropical Atlantic origin at all three levels), both models underestimate O_3 above 500 hPa by 40-60 ppb (model values of 30-50 ppb versus observations maximum values of 80-100 ppb). A previous analysis of ozone soundings and aircraft measurements at Natal suggested that increases in tropospheric ozone in the Southern Hemisphere springtime may be due to stratospheric intrusion (Logan, 1985). This is consistent with the November 2008 profiles at Natal; the models may not be capturing the intrusion of stratospheric air masses seen in the observations, indicated by upper tropospheric (> 500 hPa) layers with elevated O_3 and very low relative humidity (< 20%). On the other hand, at Paramaribo on 6 November and 25 November 2008 and at Paramaribo on 4 May 2009, when air masses at all levels were of Northern Hemisphere origin, the models reproduced the nearly constant with altitude O_3 values of 30-40 ppb.

4.3.5 Chemistry

The excess O_3 in the PBL in the models could be due to either a low deposition sink, as O_3 dry deposition velocities in the models are about half of observed values, or excessive model sensitivity to NO_x emissions, or both. Two additional simulations were conducted with WRF-Chem to evaluate the model sensitivity to these processes: (1)

doubling the calculated deposition velocity for O_3 only (2DEPVEL) and (2) halving the NO_x surface emission rates (0.5ENOx). The O_3 profiles corresponding to BARCA flights for these two simulations are also included in Figs. 12 and 14. The corresponding NO profiles from all model simulations as well as a mean profile over Amazônia from ABLE-2A are depicted in Figs. 13 and 14. The 0.5ENOx simulation reduces O_3 more than 2DEPVEL throughout the entire profile. In the dry-to-wet transition, 2DEPVEL reduces O_3 in the lower PBL by about 25%, while 0.5ENOx decreases O_3 by around 40%, and in the wet-to-dry-transition the reductions are about 10% and 30%, respectively. In general the 0.5ENOx O_3 profiles are lower than observed in the first 500 m above the surface, but they provide the best representation of the data for the north and west regions in the dry-to-wet transition. They also provide a similarly good fit as 2DEPVEL for the east, Manaus and south regions, while in the wet-to-dry transition 0.5ENOx is closer to the observed value from 0-500 m in all regions except the north. During BARCA A, NO in all WRF-Chem simulations in the north, west, and Manaus regions is 10-15 ppt from 0-500 m above the surface, increasing to a maximum of 20-50 ppt at 2 km a.g.l., and is generally lower than the ABLE-2A observations in the PBL. In the east and south, where biomass burning influence was seen, NO in 0-500 m a.g.l. increased from 20-50 ppt in the base simulation to 35-60 ppt in 2DEPVEL due to decreased O_3 and conversion of NO to NO_2, and was generally within one standard deviation of the ABLE-2A measurements in the PBL. In BARCA B, NO simulated by WRF-Chem is very low, 5-10 ppt in the entire profile, except for the west region, where a mean NO of 30 ppt is seen from 0-500 m a.g.l. This is again due to very low O_3, and for the Manaus region, where anthropogenic NO_x sources may have contributed to NO values of 20 ppt. These results suggest that adjustment of dry deposition parameterizations are needed to increase O_3 deposition velocities by about a factor of two in agreement with ground observations. Future research will compare simulated NO_x fields with observations from more recent field campaigns, as the results of these simulations also suggest that O_3 in WRF-Chem is very sensitive to NO_x emissions.

In summary, chemistry simulations of the BARCA periods with CCATT-BRAMS and WRF-Chem overestimated O_3 in the PBL by 5-10 ppb in the wet-to-dry transition (BARCA B), with background levels observed (10-20 ppb) in all regions. In the dry-to-wet transition (BARCA A), the models generally reproduced elevated O_3 levels in the northeast and southeast Amazon where biomass burning emissions of precursors led to significant enhancements of ambient O_3. However, the models overestimate O_3 in the PBL by 5-10 ppb, whereas from 2-4 km the modeled values are generally lower than observations. These discrepancies of models with observations may result from an overly-mixed (constant with altitude) profile due to overly active turbulent mixing from 1-2 km or too much downward convective transport of O_3 from 2 km to the surface, as observed by Betts et al. (2002). In addition, the models may be missing sources of O_3 and/or precursors at 3-4.5 km in the model inflow boundary conditions. The surface sink of O_3 (dry deposition) may be too low, or overestimation of NO_x sources may produce too much O_3. In the lower boundary layer, the surface sink of O_3 (dry deposition) may be too low, or overestimation of NO_x sources may produce too much O_3. Additional simulations with WRF-Chem showed that O_3 in the lower boundary layer was about twice as sensitive to increases in O_3 deposition velocity as reductions in NO_x emissions, but both simulations achieved better agreement with observations. Although NO emissions over the forest were less than half of observed values, likely due to the lack of inclusion of soil emissions, sufficient O_3 production occurred to match or exceed aircraft observations, suggesting that the model chemistry is overly NO_x-sensitive.

5 Conclusions

The BARCA campaign offered the first regional aircraft survey of O_3 in the Amazon Basin in both the dry-to-wet and wet-to-dry transition seasons. In both seasons, extremely low background O_3 values (< 20 ppb) were observed to the west and north of Manaus, and in the wet-to-dry transition low O_3 was also measured to the east and south and in the region around Manaus. These background values are the lowest observed on Earth, due to a combination of isolation from anthropogenic and biomass burning NO_x sources and O_3 deposition to the forest canopy, and the ecosystem and atmospheric chemistry is adjusted to these very low values. According to the models, the chemistry in the Amazon is very sensitive to NO_x emissions from soils, so that even a small overestimate of NO_x emissions generates too much O_3 in the PBL. However, it is likely that the model chemistry is incorrect in the PBL, because the models have about the right amount of NO_x but far too much O_3 in the PBL. Further simulations with WRF-Chem showed that the model O_3 production is very sensitive to both the O_3 deposition velocities, which were about one half of observed values, and the NO_x emissions. In polluted, VOC-sensitive conditions, approximately the correct net amount of O_3 is generated in the PBL. This suggests there is insufficient VOC reactivity in the models, since the correct amounts of O_3 deposition velocities and NO_x emissions would both decrease O_3 production. Additionally, in clean, NO_x-sensitive conditions, proportionally more O_3 is produced per unit NO_x emissions and the O_3 deposition velocities are still too low, resulting in an overestimate. Therefore, we conclude that the current model chemistry produces much more O_3 per unit NO_x than the atmosphere at very low NO_x, but may be about right in polluted conditions. In addition, simulated O_3 was lower than both the OMI/MLS total tropospheric O_3 and the BARCA observations in mid-levels, indicating that the models are missing sources at mid-levels from long-range and convective transport.

As the regional population grows in the Amazon basin, leading to increases in both urban and fire NO_x sources, this is indeed a big concern because PBL O_3 is lower in clean areas than the models predict, so that the change to polluted conditions is larger, and that the chemistry to define the path to higher NO_x conditions is poorly represented. Future modeling studies can include more complete organic chemistry and biogenic emissions, including NO emissions from soil, as well as improved representation of lightning NO_x production, dry deposition, convective transport and wet scavenging processes, to address this NO_x sensitivity. Additionally, future field campaigns in the Amazon that include aircraft observations of nitrogen oxides and hydrocarbons and ground-based measurements of NO flux from the forest canopy may allow better constraints on the Amazonian O_3 budget.

Acknowledgements

The authors are grateful to the entire BARCA team, including E. Gottlieb, V.Y. Chow, M.D.P. Longo, G.W. Santoni, F. Morais, A.C. Ribeiro, N. Jürgens, J. Steinbach, H. Chen, O. Kolle, L.V. Gatti, J.B. Miller, and the two INPE Bandeirante airplane pilots, P. Celso and D. Gramacho. We would also like to thank the GMAI group at INPE for indispensable support with the modeling and analysis, including M. Alonso, R. Braz, D. Franca, H. Lopez, R. Mello, R. Oliveira, V. Oliveira, M. Sanchez, F. Santos and R. Stockler. Many thanks to Anne Thompson, Neusa Paes Leme, Rinus Scheele, and Francis J. Schmidlin for the SHADOZ ozone sounding data. We thank B. Holben for his effort in establishing and maintaining the Manaus AERONET site. This work was supported by an IIE Fulbright Scholarship and PCI CNPQ, and the flight campaign was supported by the Max Planck Society, NASA grants NASA NNX08AP68A and NASA NNX10AR75G, FAPESP thematic project AEROCLIMA 2008/58100-2, CNPq Millennium Institute of the Large Scale Biosphere – Atmosphere Experiment in Amazonia (LBA) (CNPq Project 477575/2008-0), and MCT and INPE. Finally, we would like to express our gratitude to the three anonymous reviewers for their generous comments and revisions which greatly improved the manuscript.

References

Alonso, M. F., Longo, K., Freitas, S., Fonseca, R., Marecal, V., Pirre, M., and Klenner, L.: An urban emissions inventory for South America and its application in numerical modeling of atmospheric chemical composition at local and regional scales, Atmos. Environ., 44, 5072–5083, 2010.

Andreae, M. O., Artaxo, P., Fischer, H., Freitas, S. R., Grégoire, J.-M., Hansel, A., Hoor, P., Kormann, R., Krejci, R., Lange, L., Lelieveld, J., Lindinger, W., Longo, K., Peters, W., de Reus, M., Scheeren, B., Silva Dias, M. A. F., Stroem, J., van Velthoven, P. F. J., and Williams, J.: Transport of biomass burning smoke to the upper troposphere by deep convection in the equatorial region, Geophys. Res. Lettt., 28, 951–954, 2001.

Andreae, M. O., Artaxo, P., Brandão, C., Carswell, F. E., Ciccioli, P., da Costa, A. L., Culf, A. D., Esteves, J. L., Gash, J. H. C., Grace, J., Kabat, P., Lelieveld, J., Malhi, Y., Manzi, A. O., Meixner, F. X., Nobre, A. D., Nobre, C., Ruivo, M. d. L. P., Silva-Dias, M. A., Stefani, P., Valentini, R., von Jouanne, J., and Waterloo, M. J.: Biogeochemical cycling of carbon, water, energy, trace gases, and aerosols in Amazonia: The LBA-EUSTACH experiments, J. Geophys. Res., 107(D20), 8066, doi:10.1029/2001JD000524, 2002.

Andreae M. O., Rosenfeld, D., Artaxo, P., Costa, A. A., Frank, G. P., Longo, K. M., Silva Dias, M. A. F.: Smoking rain clouds over the Amazon, Science, 303, 1337, 2004.

Andreae, M. O., Artaxo, P., Beck, V., Bela, M., Freitas, S., Gerbig, C., Longo, K., Munger, J. W., Wiedemann, K. T., and Wofsy, S. C.: Carbon monoxide and related trace gases and aerosols over the Amazon Basin during the wet and dry-to-wet transition seasons, Atmos. Chem. Phys., 12, 6041-6065, doi:10.5194/acp-12-6041-2012, 2012.

Avery, M., Twohy, C., McCabe, D., Joiner, J., Severance, K., Atlas, E., Blake, D., Bui, T. P., Crounse, J., Dibb, J., Diskin, G., Lawson, P., McGill, M., Rogers, D., Sachse, G., Scheuer, E., Thompson, A. M., Trepte, C., Wennberg, P., Ziemke, J.: Convective distribution of tropospheric ozone and tracers in the Central American ITCZ region: Evidence from observations during TC4, J. Geophys. Res., 115, D00J21, doi:10.1029/2009JD013450, 2010.

Barth, M. C., Stuart, A. L., and Skamarock, W. C.: Numerical simulations of the July 10 STERAO/Deep Convection storm: Redistribution of soluble tracers, J. Geophys. Res., 106, 12 381–12 400, 2001.

Barth, M. C., Kim, S.-W., Wang, C., Pickering, K. E., Ott, L. E., Stenchikov, G., Leriche, M., Cautenet, S., Pinty, J.-P., Barthe, Ch., Mari, C., Helsdon, J. H., Farley, R. D., Fridlind, A. M., Ackerman, A. S., Spiridonov, V., and Telenta, B.: Cloud-scale model intercomparison of chemical constituent transport in deep convection, Atmos. Chem. Phys., 7, 4709-4731, doi:10.5194/acp-7-4709-2007, 2007.

Beck, V., Gerbig, C., Koch, T., Bela, M. M., Longo, K. M., Freitas, S. R., Kaplan, J. O., Prigent, C., Bergamaschi, P., and Heimann, M.: WRF-Chem simulations in the Amazon region during wet and dry season transitions: evaluation of methane models and wetland inundation maps, Atmos. Chem. Phys., 13, 7961-7982, doi:10.5194/acp-13-7961-2013, 2013.

Berge, E.: Coupling of wet scavenging of sulphur to clouds in a numerical weather prediction model, Tellus, 45B, 1-22, 1993.

Betts, A. K., L. V. Gatti, A. M. Cordova, M. A. F. Silva Dias, and J. D. Fuentes, Transport of ozone to the surface by convective downdrafts at night, J. Geophys. Res., 107(D20), 8046, doi:10.1029/2000JD000158, 2002.

Bond, D.W., Steiger, S., Zhang, R., Tie, X.X. and Orville, R.E.: The importance of NOx production by lightning in the tropics, Atmos. Environ., 36, 1509-1519, doi:10.1016/S1352-2310(01)00553-2, 2002.

Browell, E. V., Gregory, G. L., Harriss, R. C., and Kirchhoff, V. W. J. H.: Tropospheric ozone and aerosol distributions across the Amazon Basin, J. Geophys. Res., 93(D2), 1431–1451, doi:10.1029/JD093iD02p01431, 1988.

Browell, E. V., Fenn, M. A., Butler, C. F., Grant, W. B., Clayton, M. E., Fishman, J., Bachmeier, A. S., Anderson, B. E., Gregory, G. L., Fuelberg, H. E., Bradshaw, J. D., Sandholm, S. T., Blake, D. R., Heikes, B. G., Sachse, G. W., Singh, H. B., and Talbot, R. W., Ozone and aerosol distributions and air mass characteristics over the South Atlantic Basin during the burning season, J. Geophys. Res., 101, 24,043-24,068, 1996.

Buarque, D. C., de Paiva, R. C. D., Clarke, R. T., and Mendes, C. A. B.: A comparison of Amazon rainfall characteristics derived from TRMM, CMORPH and the Brazilian national rain gauge network, J. Geophys. Res., 116, D19105, doi:10.1029/2011JD016060, 2011.

Chen, Y., Velicogna, I., Famiglietti, J. S., and Randerson, J. T.: Satellite observations of terrestrial water storage provide early warning information about drought and fire season severity in the Amazon, J. Geophys. Res. Biogeosci., 118, 495–504, doi: 10.1002/jgrg.20046, 2013.

Chin, M., Ginoux, P., Kinne, S., Holben, B. N., Duncan, B. N., Martin, R. V., Logan, J. A., Higurashi, A., and Nakajima, T.: Tropospheric aerosol optical thickness from the

GOCART model and comparisons with satellite and sunphotometer measurements, J. Atmos. Sci. 59, 461-483, 2002.

Cordova Leal, A. M.: Gases Traço na Amazônia: Variabilidade Sazonal e Temporal de O_3, NO_x e CO em Ambientes de Pastagem e Floresta, Tese de Doutorado, Instituto de Astronomia, Geofísica e Ciências Atmosféricas da Universidade de São Paulo, 2003.

Crutzen, P. J., Delany, A. C., Greenberg, J. P., Haagenson, P., Heidt, L., Lueb, R., Polock, W., Seiler, W., Wartburg, A. F., and Zimmerman, P. R.: Tropospheric chemical composition measurements in Brazil during the dry season: J. Atmos. Chem., 2, 233-256, 1985.

Ebben, C. J., Martinez, I. S., Shrestha, M., Buchbinder, A. M., Corrigan, A. L., Guenther, A., Karl, T., Petäjä, T., Song, W. W., Zorn, S. R., Artaxo, P., Kulmala, M., Martin, S. T., Russell, L. M., Williams, J., and Geiger, F. M.: Contrasting organic aerosol particles from boreal and tropical forests during HUMPPA-COPEC-2010 and AMAZE-08 using coherent vibrational spectroscopy, Atmos. Chem. Phys., 11, 10317-10329, doi:10.5194/acp-11-10317-2011, 2011.

Fall, R., and Wildermuth, M. C.: Isoprene Synthase: From Biochemical Mechanism to Emission Algorithm, J. Geophys. Res., 103(D19), 25599-25609, doi: 10.1029/98jd00808, 1998.

Fan, S. M., Wofsy, S. C., Bakwin, P. S., Jacob, D. J., and Fitzjarrald, D. R.: Atmosphere-biosphere exchange of CO_2 and O_3 in the central Amazon forest, J. Geophys. Res., 95(D10), 16 851–16 864, 1990.

Fishman, J., and Larsen, J. C., The distribution of total ozone and stratospheric ozone in the tropics: Implications for the distribution of tropospheric ozone, J. Geophys. Res., 92, 6627-6634, 1987.

Fueglistaler S., Dessler, A. E., Dunkerton, T. J., Folkins, I., Fu, Q., and Mote, P. W.: Tropical tropopause layer, Rev. Geophys., 47, RG1004, doi:10.1029/2008RG000267, 2009.

Freitas, S. R., Silva Dias, M. A. F., Silva Dia, P. L., Longo, K. M., Artaxo, P., Andreae, M. O., and Fischer, H.: A convective kinematic trajectory technique for low-resolution atmospheric models, J. Geophys. Res., 105, D19, 24, 375-24, 386, doi:10.1029/2000JD900217, 2000.

Freitas, S., Longo, K., Silva Dias, M., Silva Dias, P., Chatfield, R., Prins, E., Artaxo, P., Grell, G. and Recuero, F.: Monitoring the transport of biomass burning emissions in

South America, Environ. Fluid Mech., DOI: 10.1007/s10652-005-0243-7, 5(1-2), 135-167, 2005.

Freitas, S. R., Longo, K. M., Chatfield, R., Latham, D., Silva Dias, M. A. F., Andreae, M. O., Prins, E., Santos, J. C., Gielow, R., and Carvalho Jr., J. A.: Including the sub-grid scale plume rise of vegetation fires in low resolution atmospheric transport models, Atmos. Chem. Phys., 7, 3385-3398, doi:10.5194/acp-7-3385-2007, 2007.

Freitas, S. R., Longo, K. M., Silva Dias, M. A. F., Chatfield, R., Silva Dias, P., Artaxo, P., Andreae, M. O., Grell, G., Rodrigues, L. F., Fazenda, A., and Panetta, J.: The Coupled Aerosol and Tracer Transport model to the Brazilian developments on the Regional Atmospheric Modeling System (CATT-BRAMS) - Part 1: Model description and evaluation, Atmos. Chem. Phys., 9, 2843-2861, 2009.

Freitas, S. R., Longo, K. M., Alonso, M. F., Pirre, M., Marecal, V., Grell, G., Stockler, R., Mello, R.F., Sanchez Gacita, M.: PREP-CHEM-SRC-1.0: a preprocessor of trace gas and aerosol emission fields for regional and global atmospheric chemistry models, Geosci. Model Dev., 4, 419-433, 2011.

Gallardo, L., Alonso, M., Andrade, M. F., Carvalho, V. S. B., Behrentz, E., Vasconcellos, P. C., D'Angiola, A., Dawidowski, L., Freitas, S., Gómez, D., Longo, K. M., Martins, M., Mena, M., Matus, P., Osses, A., Osses, M., Rojas, N., Saide, P., Sánchez-Ccoyllo, O., and Toro, M. V.: South America, in IGAC Report on Megacity Air Pollution and Climate, 2010.

Garcia-Montiel, D. C., Steudler, P. A., Piccolo, M., Neill, C., Melillo, J., Cerri, C. C.: Nitrogen oxide emissions following wetting of dry soils in forest and pastures in Rondônia, Brazil, Biogeochemistry, 64(3), 319-336, 2003.

Gevaerd, R.: Estudo da Redistribuição 3-D de Gases e Aerossóis de Queimadas em Roraima 1998, Master's thesis, University of São Paulo, 2005.

Gevaerd, R. and S. R. Freitas: Estimativa operacional da umidade do solo para iniciação de modelos de previsão numérica da atmosfera. Parte I: Descrição da metodologia e validação. Revista Brasileira de Meteorologia, 21(3), 59-73, 2006.

Gevaerd, R., Freitas, S., and Longo, K.: Numerical simulation of biomass burning emission and transport during 1998 Roraima fires, in: International Conference on Southern Hemisphere Meteorology and Oceanography (ICSHMO), 8, Proceedings, Foz do Iguaçu, INPE, São José dos Campos, 2006, 883–889, CD-ROM, ISBN 85-17-00023-4, 2006.

Guenther, A., Karl, T., Harley, P., Wiedinmyer, C., Palmer, P. I., and Geron, C.: Estimates of global terrestrial isoprene emissions using MEGAN (Model of Emissions of Gases and Aerosols from Nature), Atmos. Chem. Phys., 6, 3181–3210, doi:10.5194/acp-6-3181-2006, 2006.

Grell, G. A., and D. Dévényi, A generalized approach to parameterizing convection combining ensemble and data assimilation techniques, Geophys. Res. Lett., 29(14), doi:10.1029/2002GL015311, 2002.

Grell, G. A., Peckham, S. E., Schmitz, R., McKeen, S. A., Frost, G., Skamarock, W. C., and Eder, B.: Fully coupled online chemistry within the WRF model, Atmos. Environ., 39, 6957– 6975, 2005.

Harriss, R. C., et al.: The Amazon Boundary Layer Experiment (ABLE 2A): dry season 1985, J. Geophys. Res., 93(D2), 1351–1360, doi:10.1029/JD093iD02p01351, 1988.

Harriss, R. C., Garstang, M., Wofsy, S. C., Beck, S. M., Bendura, R. J., Coelho, J. R. B., Drewry, J. W., Hoell, J. M., Matson, P. A., McNeal, R. J., Molion, L. C. B., Navarro, R. L., Rabine, V., and Snell, R. L.: The Amazon Boundary Layer Experiment: Wet Season 1987, J. Geophys. Res., 95, 16721–16736, 1990.

Jacob, D. J., and Wofsy, S. C.: Photochemistry of biogenic emissions over the Amazon forest, J. Geophys. Res., 93(D2), 1477–1486, doi:10.1029/JD093iD02p01477, 1988.

Janjić, Z. I.,: The step-mountain eta coordinate model: further developments of the 445 convection, viscous sublayer and turbulence closure schemes, Mon. Wea. Rev., 122, 446 927-945, 1994.

Kaplan, W. A., Wofsy, S. C., Keller, M., and Da Costa, J. M.: Emission of NO and deposition of O_3 in a tropical forest system, J. Geophys. Res., 93(D2), 1389–1395, doi:10.1029/JD093iD02p01389, 1988.

Karl, T., Guenther, A., Yokelson, R. J., Greenberg, J., Potosnak, M., Blake, D.R., and Artaxo, P.: The tropical forest and fire emissions experiment: Emission, chemistry, and transport of biogenic volatile organic compounds in the lower atmosphere over Amazonia, J. Geophys. Res. 112, D18302, 2007.

Kaufman, Y., Hobbs, P. V., Kirchhoff, V. W., Artaxo, P., Remer, L., Holben, B. N., King, M. D., Prins, E. M., Ward, D. E., Longo, K. M., Mattos, L. F., Nobre, C. A., Spinhirne, J., Thompson, A. M., Gleason, J. F., and Christopher, S. A.: Smoke, Clouds, and Radiation-Brazil (SCAR-B) experiment, J. Geophys. Res., 103(D24), 31783–31808, doi:10.1029/98JD02281, 1998.

Kawanishi, T., Kuroiwa, H., Kojima, M., Oikawa, K., Kozu, T., Kumagai, H., Okamoto, K., Okumura, M., Nakatsuka, H., and Nishikawa, K.: TRMM precipitation radar, Remote Sens. Appl.: Earth Atmos. Oceans, 25, 969–972, 2000.

Kirchhoff, V. W. J. H., da Silva, I. M. O., and Browell, E. V., Ozone measurements in Amazonia: Dry season versus wet season: J. Geophys. Res., 95, 16,913-16,926, 1990.

Kirkman, G. A., Gut, A., Ammann, C., Gatti, L. V., Cordova, A. M., Moura, M. A. L., Andreae, M. O., and Meixner, F. X.: Surface exchange of nitric oxide, nitrogen dioxide, and ozone at a pasture in Rondonia, Brazil, J. Geophys. Res., 107(D20), 8083, doi:10.1029/2001JD000523, 2002.

Koren, V., Schaake, J., Mitchell, K., Duan, Q.-Y. and Chen, F.: A parameterization of snowpack and frozen ground intended for NCEP weather and climate models. J. Geophys. Res., 104, 19569-19585, 1999.

Kuhn, U., Ganzeveld, L., Thielmann, A., Dindorf, T., Welling, M., Sciare, J., Roberts, G., Meixner, F. X., Kesselmeier, J., Lelieveld, J., Ciccioli, P., Lloyd, J., Trentmann, J., Artaxo, P., and Andreae, M. O., Impact of Manaus City on the Amazon Green Ocean atmosphere: Ozone production, precursor sensitivity and aerosol load, Atmos. Chem. Phys., 10, 9251–9282, 2010.

Kummerow, C., Barnes, W., Kozu T., Shiue, J., and Simpson, J.: The Tropical Rainfall Measuring Mission (TRMM) sensor package, J. Atmos. Ocean. Tech., Boston, 15(3), 809–816, 1998.

Lelieveld, J., Butler, T. M., Crowley, J. N., Dillon, T. J., Fischer, H., Ganzeveld, L., Harder, H., Lawrence, M. G., Martinez, M., Taraborrelli, D., and Williams, J.: Atmospheric oxidation capacity sustained by a tropical forest, Nature, 452, 737-740, 2008.

Logan, J.A.: Tropospheric ozone: Seasonal behavior, trends, and anthropogenic influence, J. Geophys. Res., 90, 10463-10482, 1985.

Logan, J. A.: An analysis of ozonesonde data for the troposphere: Recommendations for testing 3-D models and development of a gridded climatology for tropospheric ozone, J. Geophys. Res., 104, 16,115– 16,149, 1999.

Longo, K. M., Thompson, A. M., Kirchhoff, V. W. J. H., Remer, L. A., de Freitas, S. R., Dias, M. A. F. S., Artaxo, P., Hart, W., Spinhirne, J. D., and Yamasoe, M. A.: Correlation between smoke and tropospheric ozone concentration in Cuiabá during Smoke, Clouds, and Radiation-Brazil (SCAR-B), J. Geophys. Res., 104(D10), 12113–12129, doi:10.1029/1999JD900044, 1999.

Longo, K. M., Freitas, S. R., Andreae, M. O., Yokelson, R., Artaxo, P., Biomass burning in Amazonia: emissions, long-range transport of smoke and its regional and remote impacts, in Keller, M., Bustamante, M., Gash, J., and Silva Dias, P., ed., Amazonia and Global Change, AGU Geophysical Monograph Series, Washington, D.C., v. 186, 2009.

Longo, K. M., Freitas, S. R., Pirre, M., Marécal, V., Rodrigues, L. F., Panetta, J., Alonso, M. F., Rosário, N. E., Moreira, D. S., Gácita, M. S., Arteta, J., Fonseca, R., Stockler, R., Katsurayama, D. M., Fazenda, A., and Bela, M.: The chemistry CATT–BRAMS model (CCATT–BRAMS 4.5): a regional atmospheric model system for integrated air quality and weather forecasting and research, Geosci. Model Dev., 6, 1389-1405, doi:10.5194/gmd-6-1389-2013, 2013.

Martin, S. T., Andreae, M. O., Althausen, D., Artaxo, P., Baars, H., Borrmann, S., Chen, Q., Farmer, D. K., Guenther, A., Gunthe, S. S., Jimenez, J. L., Karl, T., Longo, K., Manzi, A., Müller, T., Pauliquevis, T., Petters, M. D., Prenni, A. J., Pöschl, U., Rizzo, L. V., Schneider, J., Smith, J. N., Swietlicki, E., Tota, J., Wang, J., Wiedensohler, A., and Zorn, S. R.: An overview of the Amazonian Aerosol Characterization Experiment 2008 (AMAZE-08), Atmos. Chem. Phys., 10, 11415-11438, doi:10.5194/acp-10-11415-2010, 2010.

Mellor, G. L. and Yamada, T.: Development of a turbulence closure model for geophysical fluid problems, Rev. Geophys. Space Phys., 20, 851–875, 1982.

Morton, D. C., Le Page, Y., DeFries, R., Collatz, G. J., and Hurtt, G. C.: Understorey fire frequency and the fate of burned forests in southern Amazonia, Phil. Trans. R. Soc. B, 368(1619), doi: 10.1098/rstb.2012.0163, 2013.

National Research Council, 1991. Rethinking the Ozone Problem in Urban and Region-al Air Pollution. National Academy Press, Washington, DC, 500pp.

Reich, P. B. and Amundson, R. G.: Ambient levels of ozone reduce net photosynthesis in tree and crop species, Science, 230, 566–570, doi:10.1126/science.230.4725.566, 1985.

Rinne, H. J. I., Guenther, A.B., Greenberg, J.P., and Harley, P.C.: Isoprene and monoterpene fluxes measured above Amazonian rainforest and their dependence on light and tempera-ture, Atmos. Environ., 36(14), 2421–2426, doi:10.1016/S1352-2310(01) 00523-4, 2002.

Rosário, N. M. E. Variability of aerosol optical properties over South America and the impacts of direct radiative effect of aerosols from biomass burning. 2011. Thesis (PhD).

Institute of Astronomy, Geophysics and Atmospheric Sciences, University of São Paulo, São Paulo, 2011 (in Portuguese).

Rosário N. E., K. M. Longo, S. R. Freitas, M. A. Yamasoe, and R. M. Fonseca. Modeling South America regional smoke plume: aerosol optical depth variability and shortwave surface forcing, Atmos. Chem. Phys., 13, 2923-2938, doi:10.5194/acp-13-2923-2013, 2013.

Rummel, U., Ammann, C., Kirkman, G. A., Moura, M. A. L., Foken, T., Andreae, M. O., and Meixner, F. X., Seasonal variation of ozone deposition to a tropical rainforest in southwest Amazonia, Atmos. Chem. Phys., 7, 5415-5435, 2007.

Seinfeld, J. H. and Pandis, S. N.: Atmospheric Chemistry and Physics: From Air Pollution to Climate Change, 2nd edition, J. Wiley, New York, 2006.

Sestini, M., Reimer, E., Valeriano, D., Alvalá , R., Mello, E., Chan, C., and Nobre, C.: Mapa de cobertura da terra da Amazônia legal para uso em modelos meteorológicos, Anais XI Simpósio Brasileiro de Sensoriamento Remoto, 2901–2906, 2003.

Sigler, J. M., Fuentes, J. D., Heitz, R. C., Garstang, M., and Fisch, G.: Ozone dynamics and deposition processes at a deforested site in the Amazon Basin, Ambio, 31(1), 21–27, 2002.

Silva, C. M. S., Freitas, S.R., Gielow, R., and Barros, S.S.: Evaluation of high-resolution precipitation estimate over the Amazon Basin, Atmos. Sci. Let., 10, 273–278, 2009.

Silva, C. M. S., Freitas, S. R., and Gielow, R.: Numerical simulation of the diurnal cycle of rainfall in SW Amazon Basin during the 1999 rainy season: the role of convective trigger function, Theor. Appl. Climatol., 109, 473, 2012.

Stockwell, D. Z., Giannakopoulos, C., Plantevin, P.-H., Carver, G. D., Chipperfield, M. P., Law, K. S., Pyle, J. A., Shallcross, D. E., and Wang, K.-Y.: Modeling NOx from lightning and its impact on global chemical fields, Atmos. Environm., 33(27), 4477-4493, 1999.

Stockwell, W. R., Kirchner, F., and Kuhn, M.: A new mechanism for regional chemistry modeling, J. Geophys. Res., 102, 25847–25879, 1997.

Thompson, A. M., Pickering, K. E., McNamara, D. P., Schoeberl, M. R., Hudson, R. D., Kim, J. H., Browell, E. V., Kirchhoff, V. W. J. H., and Nganga, D.: Where did tropospheric ozone over southern Africa and the tropical Atlantic come from in October

1992? Insights from TOMS, GTE TRACE A, and SAFARI 1992, J. Geophys. Res., 101(D19), 24251–24278, doi:10.1029/96JD01463, 1996.

Thompson, A.M., Witte, J. C., McPeters, R. D., Oltmans, S. J., Schmidlin, F. J., Logan, J. A., Fujiwara, M., Kirchhoff, V. W. J. H., Posny, F., Coetzee, G. J. R., Hoegger, B., Kawakami, S., Ogawa, T., Johnson, B. J., Vömel, H., and Labo, G.:Southern Hemisphere Additional Ozonesondes (SHADOZ) 1998-2000 tropical ozone climatology 1. Comparison with Total Ozone Mapping Spectrometer (TOMS) and ground-based measurements, J. Geophys. Res., 108, 8238, doi:10.1029/2001JD000967, 2003.

Thompson, A.M., Witte, J. C., Oltmans, S. J., Schmidlin, F. J., Logan, J. A., Fujiwara, M., Kirchhoff, V. W. J. H., Posny, F., Coetzee, G. J. R., Hoegger, B., Kawakami, S., Ogawa, T., Fortuin, J. P. F., and Kelder, H. M.: Southern Hemisphere Additional Ozonesondes (SHADOZ) 1998-2000 tropical ozone climatology 2. Tropospheric variability and the zonal wave-one, J. Geophys. Res., 108, 8241, doi:10.1029/2002JD002241, 2003.

Thompson, A. M., Witte, J.C., Smit, H.G.J., Oltmans, S.J., Johnson, B.J., Kirchhoff, V.W.J H., and Schmidlin, F.J.: Southern Hemisphere Additional Ozonesondes (SHADOZ) 1998-2004 tropical ozone climatology: 3. Instrumentation, station-to-station variability, and evaluation with simulated flight profiles, J. Geophys. Res., 112, D03304, doi:10.1029/2005JD007042, 2007.

Toon, O. B., Starr, D. O., Jensen, E. J., Newman, P. A., Platnick, S., Schoeberl, M. R.,Wennberg, P. O., Wofsy, S. C., Kurylo, M. J., Maring, H., Jucks, K. W., Craig, M. S., Vasques, M. F., Pfister, L., Rosenlof, K. H., Selkirk, H. B., Colarco, P. R., Kawa, S. R., Mace, G. G., Minnis, P., and Pickering, K. E.: Planning, implementation, and first results of the Tropical Composition, Cloud and Climate Coupling Experiment (TC4), J. Geophys. Res., 115, D00J04, doi:10.1029/2009JD013073, 2010.

Torres, A. L., and Buchan, H.: Tropospheric nitric oxide measurements over the Amazon Basin, J. Geophys. Res., 93(D2), 1396–1406, doi:10.1029/JD093iD02p01396, 1988.

von Randow, C., Manzi, A. O., Kruijt, B., de Oliveira, P. J., Zanchi, F. B., Silva, R. L., Hodnett, M. G., Gash, J. H. C., Elbers, J. A. Waterloo, M. J., Cardoso, F. L., and Kabat, P.: Comparative measurements and seasonal variations in energy and carbon exchange over forest and pasture in South West Amazonia, Theor. Appl. Climatol., 78, 5–26 (2004), DOI 10.1007/s00704-004-0041-z, 2004.

Walko, R. L., Band, L. E., Baron, J., Kittel, T.G.F., Lammers, R., Lee, T. J., Ojima, D., Pielke, R. A., Taylor, C., Tague, C., Tremback, C. J., and Vidale, P.L.: Coupled atmosphere-biophysics hydrology models for environmental modeling, J. Appl. Meteor., 39, 931-944, 2000.

Wesley, M. L.: Parameterization of surface resistance to gaseous dry deposition in regional numerical models, Atmos. Environ., 16, 1293–1304, 1989.

Zhang, L., Jacob, D. J., Liu, X., Logan, J. A., Chance, K., Eldering, A., and Bojkov, B. R.: Intercomparison methods for satellite measurements of atmospheric composition: application to tropospheric ozone from TES and OMI, Atmos. Chem. Phys., 10, 4725-4739, 2010.

Zhou, J., Swietlicki, E., Hansson, H. C., and Artaxo, P.: Submicrometer aerosol particle size distribution and hygroscopic growth measured in the Amazon rain forest during the wet-to-dry transition season, J. Geophys. Res., 107(D20), 8055, doi:10.1029/2000JD000203, 2002.

Ziemke, J. R., Chandra, S., Duncan, B. N., Froidevaux, L., Bhartia, P. K., Levelt, P. F. and Waters, J. W.: Tropospheric ozone determined from Aura OMI and MLS: Evaluation of measurements and comparison with the Global Modeling Initiative's Chemical Transport Model, J. Geophys. Res., 111, D19303, doi:10.1029/2006JD007089, 2006.

Ziemke, J. R., Joiner, J., Chandra, S., Bhartia, P. K., Vasilkov, A., Haffner, D. P., Yang, K., Schoeberl, M. R., Froidevaux, L., and Levelt, P. F.:Ozone mixing ratios inside tropical deep convective clouds from OMI satellite measurements, Atmos. Chem. Phys., 9, 573–583, 2009.

	CCATT-BRAMS	**WRF-Chem**
Short/longwave radiation	Based on CARMA	RRTMG
Cloud microphysics	Single moment bulk	WSM-5
Deep/shallow convection	Grell and Dévényi (GD)	Grell 3D
Trace gas chemistry	RACM	RACM
Photolysis	F-TUV	F-TUV
Aerosol scheme	Smoke aerosol	GOCART
Wet deposition	convective and grid scales	convective scale only

Table 1. CCATT-BRAMS and WRF-Chem physics and chemistry options for the BARCA simulations.

	Nov. 2008			May 2009		
Region	**TRMM 3B43**	**CCATT-BRAMS**	**WRF-Chem**	**TRMM 3B43**	**CCATT-BRAMS**	**WRF-Chem**
Amazon	0.24	0.22	0.51	0.20	0.15	0.40
Northeast	0.12	0.07	0.08	0.37	0.23	0.49
Southeast	0.19	0.11	0.24	0.10	0.06	0.07

Table 2. Monthly mean precipitation (mm h^{-1}) for TRMM 3B43, CCATT-BRAMS and WRF-Chem models for three regions: the Amazon (15°S – 10°N, 50°W – 80°W), northeast Brazil (15°S – 0°N, 35°W – 50°W), and southeast South America (15°S – 35°S, 35°W – 65°W).

			Oct-Nov 2008			May-Apr 2009	
			CCATT-BRAMS	**WRF-Chem**		**CCATT-BRAMS**	**WRF-Chem**
T (K)	*Mean Obs.*	*295.97*			*293.89*		
	RMSE		2.30	2.81		1.70	2.44
	Bias		1.04	-2.42		-0.06	-2.28
T_d (K)	*Mean Obs.*	*289.26*			*288.49*		
	RMSE		2.68	1.72		1.76	1.67
	Bias		-1.92	-0.81		-0.99	-0.83
Wind Spd.	*Mean Obs.*	*3.00*			*2.59*		
(m s-1)	RMSE		1.41	1.33		1.15	1.00
	Bias		-0.60	0.16		-0.51	0.07
Sfc. Press.	*Mean Obs.*	*1013.17*			*1016.09*		
(hPa)	RMSE		2.16	1.43		1.09	1.34
	Bias		-2.01	-1.02		-0.79	-1.17
Precip. TRMM	Mean Obs.	*0.49*			*0.62*		
(mm h^{-1})	RMSE		2.42	4.50		3.03	7.12
	Bias		0.28	3.47		0.25	5.84

Table 3. Values of RMSE and bias for CCATT-BRAMS and WRF-Chem simulations for 26 METAR and 52 SYNOP stations in the Amazon Basin for BARCA A (October-November 2008) and BARCA B (April-May 2009).

PBL Height (km)		Method	Forest TKE	Forest Theta	Forest WRF MYNN	Pasture TKE	Pasture Theta	Pasture WRF MYNN
BARCA A (Nov. 2008)	CCATT-BRAMS	Mean	**1.103**	**1.610**	---	**1.143**	**1.636**	---
		Std. Dev.	0.621	0.646	---	0.581	0.640	---
	WRF-Chem	Mean	**1.211**	**1.131**	**0.983**	**1.258**	**1.087**	**0.991**
		Std. Dev.	0.655	0.390	0.423	0.665	0.470	0.455
BARCA B (May 2009)	CCATT-BRAMS	Mean	**0.628**	**1.067**	---	**0.669**	**1.049**	---
		Std. Dev.	0.515	0.554	---	0.527	0.564	---
	WRF-Chem	Mean	**0.828**	**0.922**	**0.815**	**0.845**	**0.933**	**0.766**
		Std. Dev.	0.443	0.336	0.288	0.432	0.282	0.272

Table 4. PBL height at 21:00 UTC (17:00 LT) estimated from CCATT-BRAMS and WRF-Chem using methods based on Turbulent Kinetic Energy (TKE) and theta (θ) and the diagnostic from the WRF MYNN PBL scheme.

Site		Dry Season Observed	Dry Season CCATT-BRAMS	Dry Season WRF-Chem	Wet Season Observed	Wet Season CCATT-BRAMS	Wet Season WRF-Chem
RBJ (forest)	Flux	-5.69	-2.43	-3.25	-2.93	-1.59	-2.39
	v_d	0.6	0.3	0.5	1.2	0.4	0.8
FNS (pasture)	Flux	-4.68	-3.06	-2.49	-2.04	-2.07	-2.04
	v_d	0.6	0.4	0.4	0.7	0.4	0.7
RD (forest)	Flux				-1.82	-1.63	-2.68
	v_d				1.6	0.4	0.6

Table 5. Average O_3 dry deposition flux (nmol m^{-2} s^{-1}) and daytime (11:00-21:00 UTC) median deposition velocity (cm s^{-1}) in the dry and wet seasons (Rummel et al., 2007), and WRF-Chem and CCATT-BRAMS simulations from November 2008 (dry-to-wet transition) and May 2009 (wet-to-dry transition) for Reserva Biológica Jarú (RBJ), Fazenda Nossa Senhora (RNS) and Reserva Ducke (RD).

	BARCA A (Nov. 2008)					*BARCA B (May 2009)*				
Region	**Longitude**		**Latitude**		**Days**	**Longitude**		**Latitude**		**Days**
west	-60.06	-54.24	-12.00	-3.03	29, 30	-61.16	-59.46	-3.71	-2.39	28
north	-62.00	-59.11	-3.04	2.89	23	-61.81	-60.00	-3.04	3.71	19
around Manaus	-61.52	-58.50	-4.39	1.00	16, 22	-62.14	-60.00	-4.07	-2.16	15, 17
east	-108.73	-48.45	-3.04	-1.33	18, 19	-60.34	-44.82	-4.39	0.14	21, 22, 23, 26
south	-67.69	-60.01	-3.40	0.12	25, 26	-63.93	-60.01	-8.77	-3.04	27

Table 6. Longitude and latitude bounds and dates for each region of the BARCA A and B campaigns.

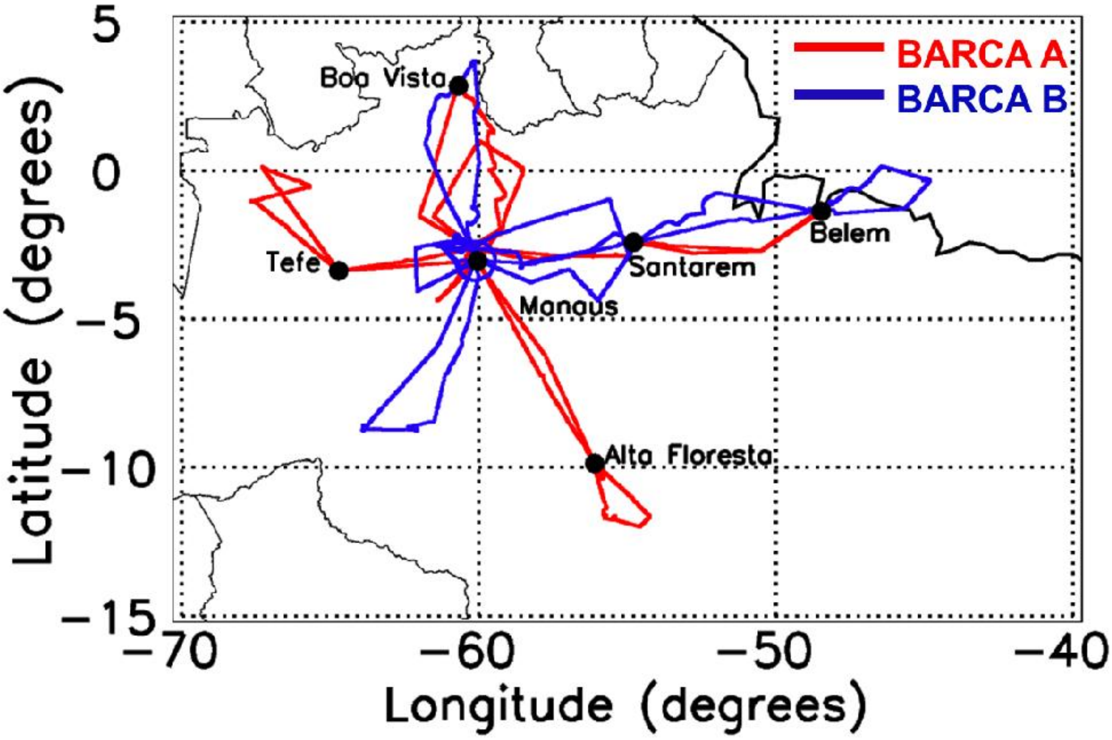

Figure 1. Flight tracks during BARCA.

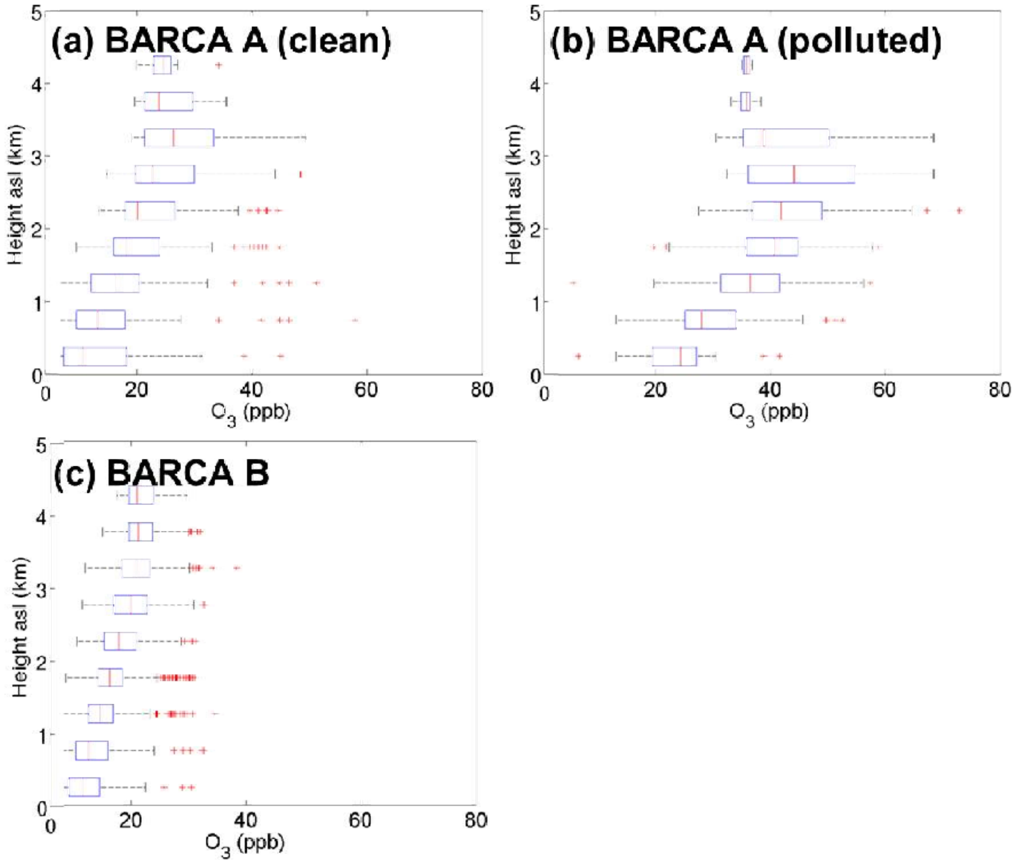

Figure 2. O_3 observations during (a) BARCA A, clean conditions (West, North and around Manaus regions), (b) BARCA A, polluted conditions (East and South regions) and (c) BARCA B. The central mark is the median, the edges of the box are the 25th and 75th percentiles, the whiskers extend to the most extreme data points not considered outliers (as defined by Matlab) and outliers are plotted individually as red plusses. Values are drawn as outliers if their values exceed $q_3 + w(q_3 - q_1)$ or are less than $q_1 - w(q_3 - q_1)$, where q_1 and q_3 are the 25th and 75th percentiles, respectively, and w is the maximum whisker length with the default value of 1.5. For normally distributed data, the whiskers encompass from approximately the 2.7 to 99.3 percentiles.

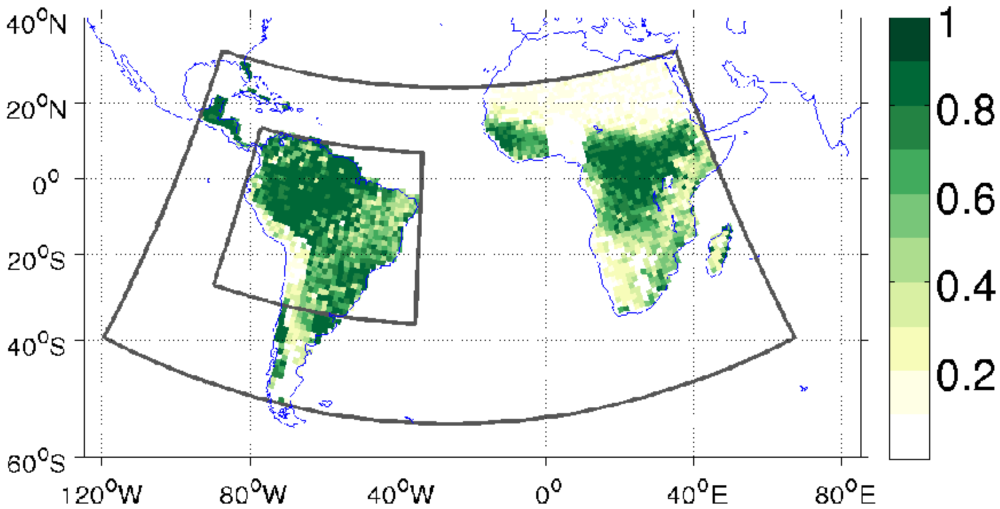

Figure 3. Land surface albedo (fraction) and locations of the coarse (140 km resolution) and nested (35 km resolution) domains for WRF-Chem simulations.

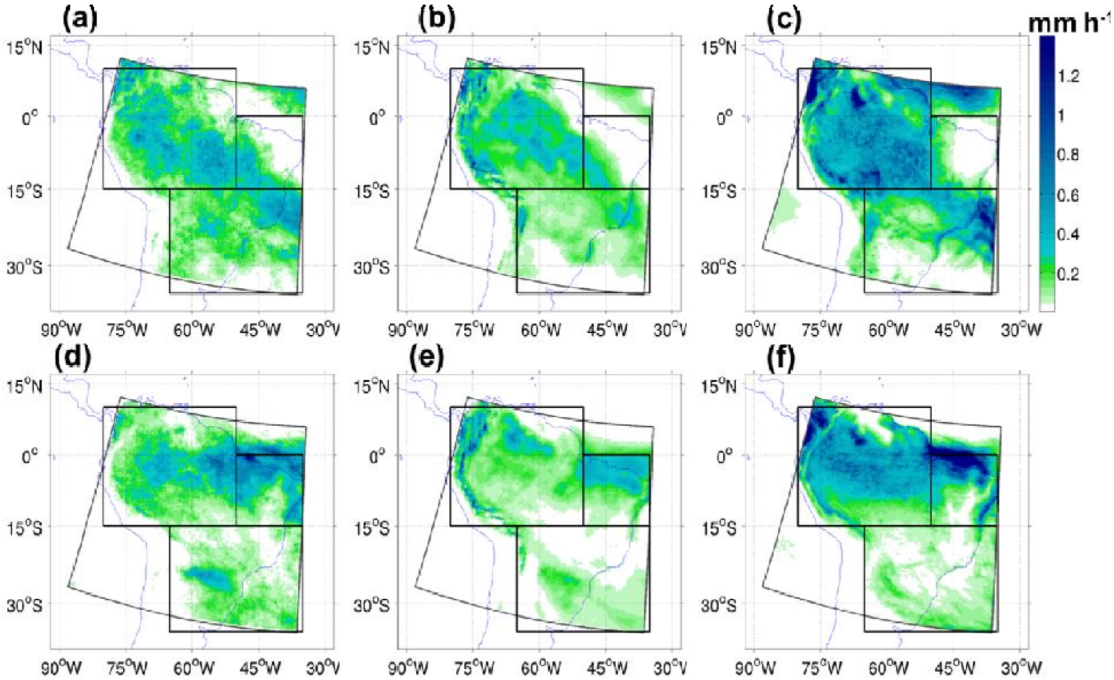

Figure 4. Monthly mean precipitation (mm h^{-1}) on the 35-km resolution domain (dark gray line) for November 2008 from (a) TRMM 3B43, (b) CCATT-BRAMS and (c) WRF-Chem and for May 2009 from (c) TRMM 3B43, (d) CCATT-BRAMS and (f) WRF-Chem. The subregions for precipitation comparison are indicated by black lines.

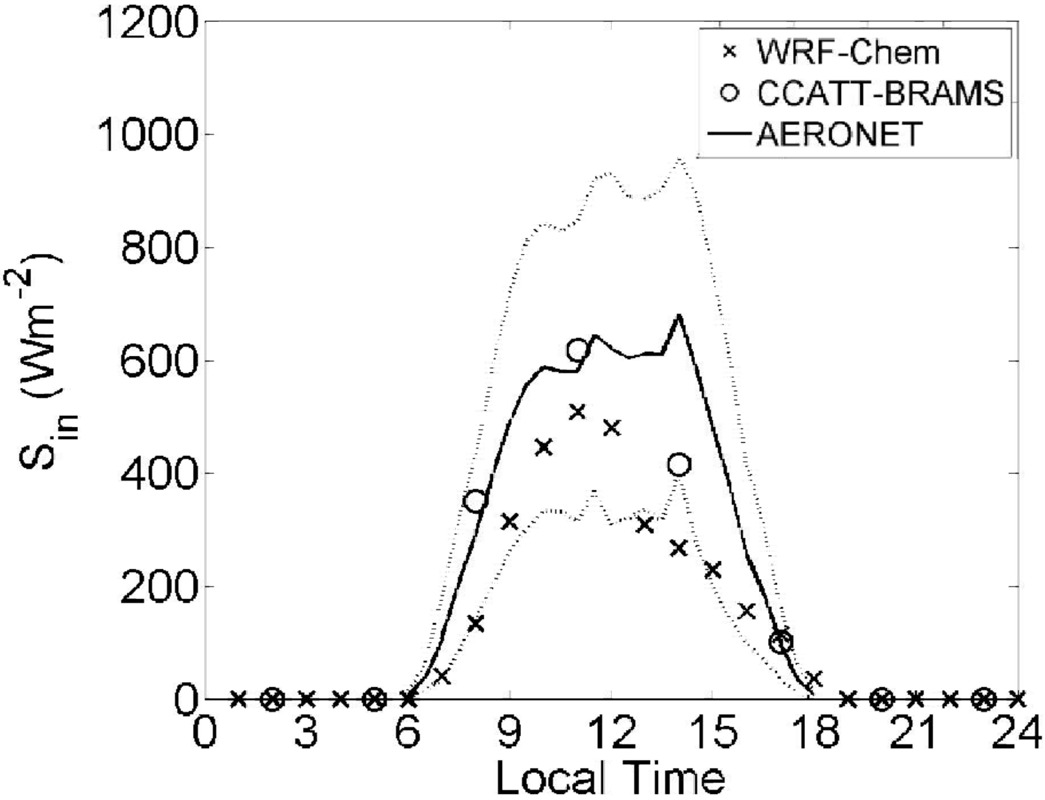

Figure 5. Mean daily cycle of surface incident shortwave radiation from the Manaus AERONET site (solid line, dotted line denotes one standard deviation), WRF-Chem (crosses) and CCATT-BRAMS (circles) for the BARCA A period (October-November 2008).

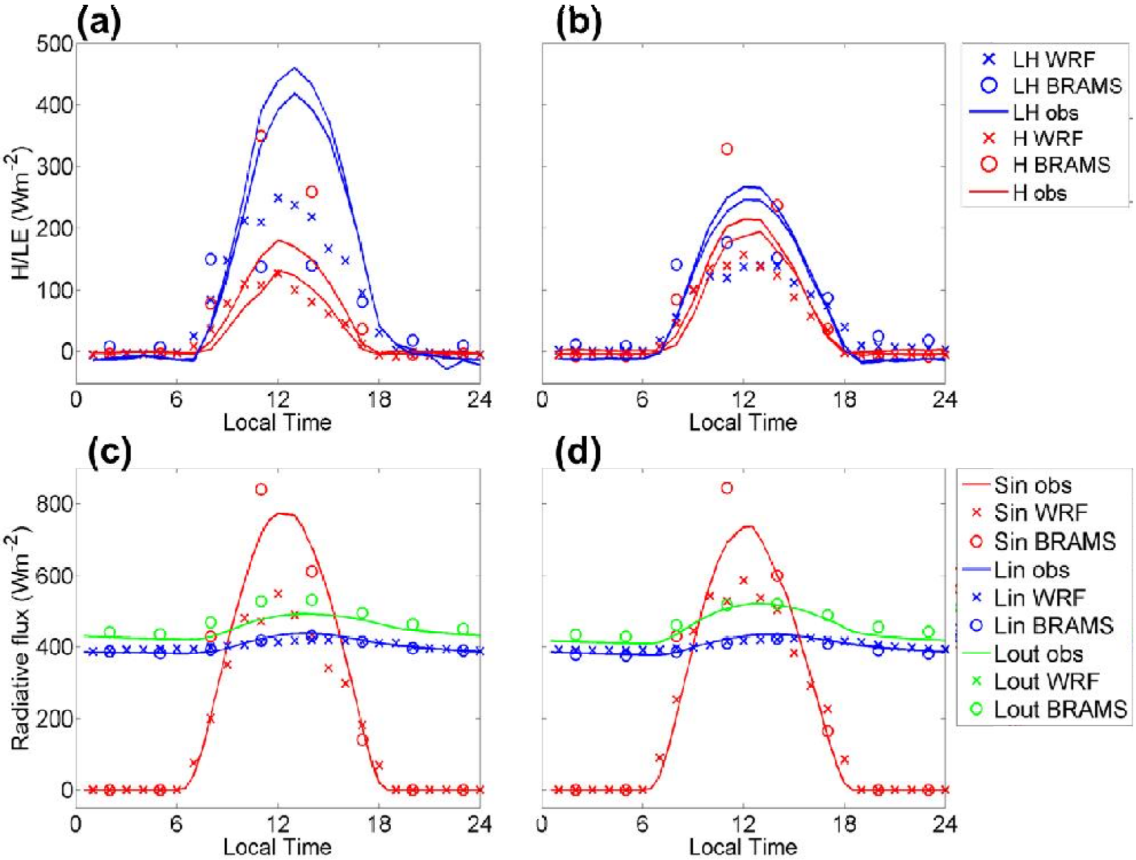

Figure 6. Mean daily cycles of surface (a) latent (LE) and sensible (H) heat and (c) incident shortwave (S_{in}) and incoming (L_{in}) and outgoing (L_{out}) longwave radiation fluxes for a forest site and (b) heat and (d) radiation fluxes for a pasture site, comparing observations (solid lines) from von Randow et al. (2004) for the dry-to-wet transition season (July-September 1999-2000) and from WRF-Chem (crosses) and CCATT-BRAMS (circles) for the BARCA A period (October-November 2008).

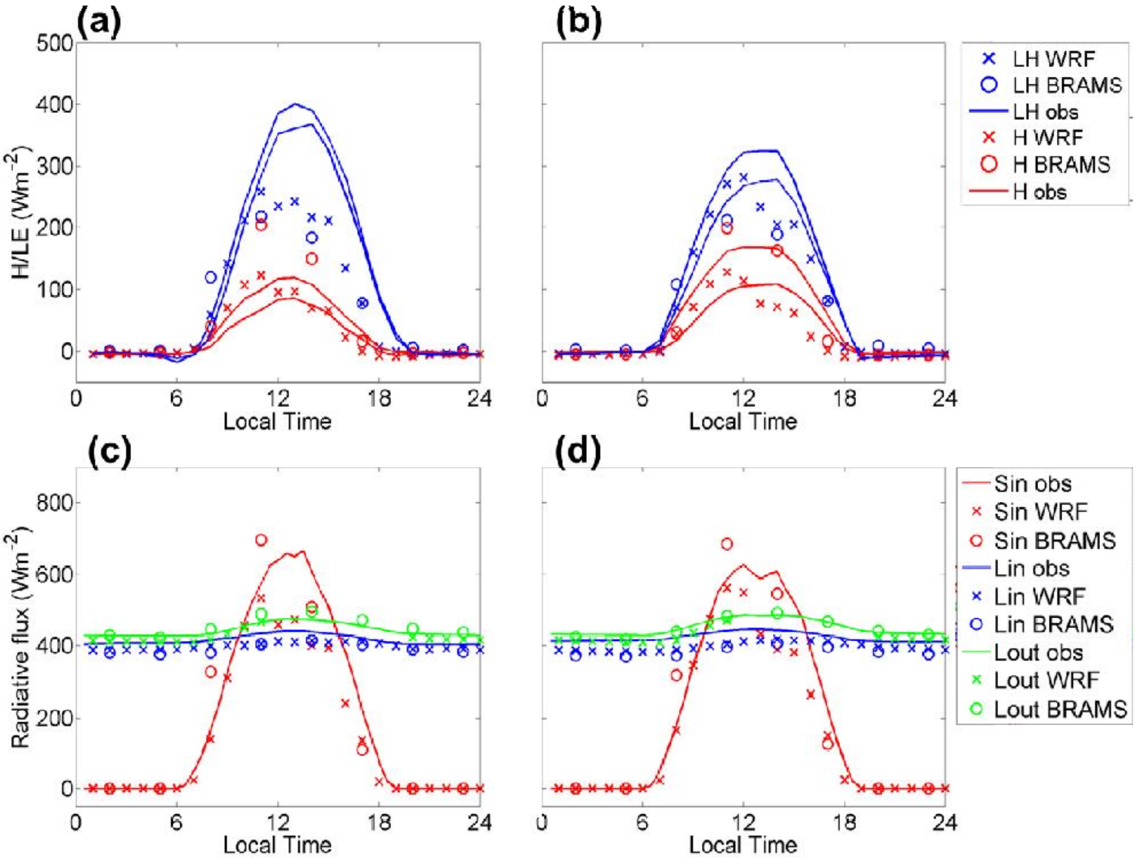

Figure 7. Mean daily cycles of surface (a) latent (LE) and sensible (H) heat and (c) incident shortwave (S_{in}) and incoming (L_{in}) and outgoing (L_{out}) longwave radiation fluxes for a forest site and (b) heat and (d) radiation fluxes for a pasture site, comparing observations (solid lines) from von Randow et al. (2004) for the wet-to-dry transition season (February-March 1999, January-March 2000) and from WRF-Chem (crosses) and CCATT-BRAMS (circles) for the BARCA B period (April-May 2009).

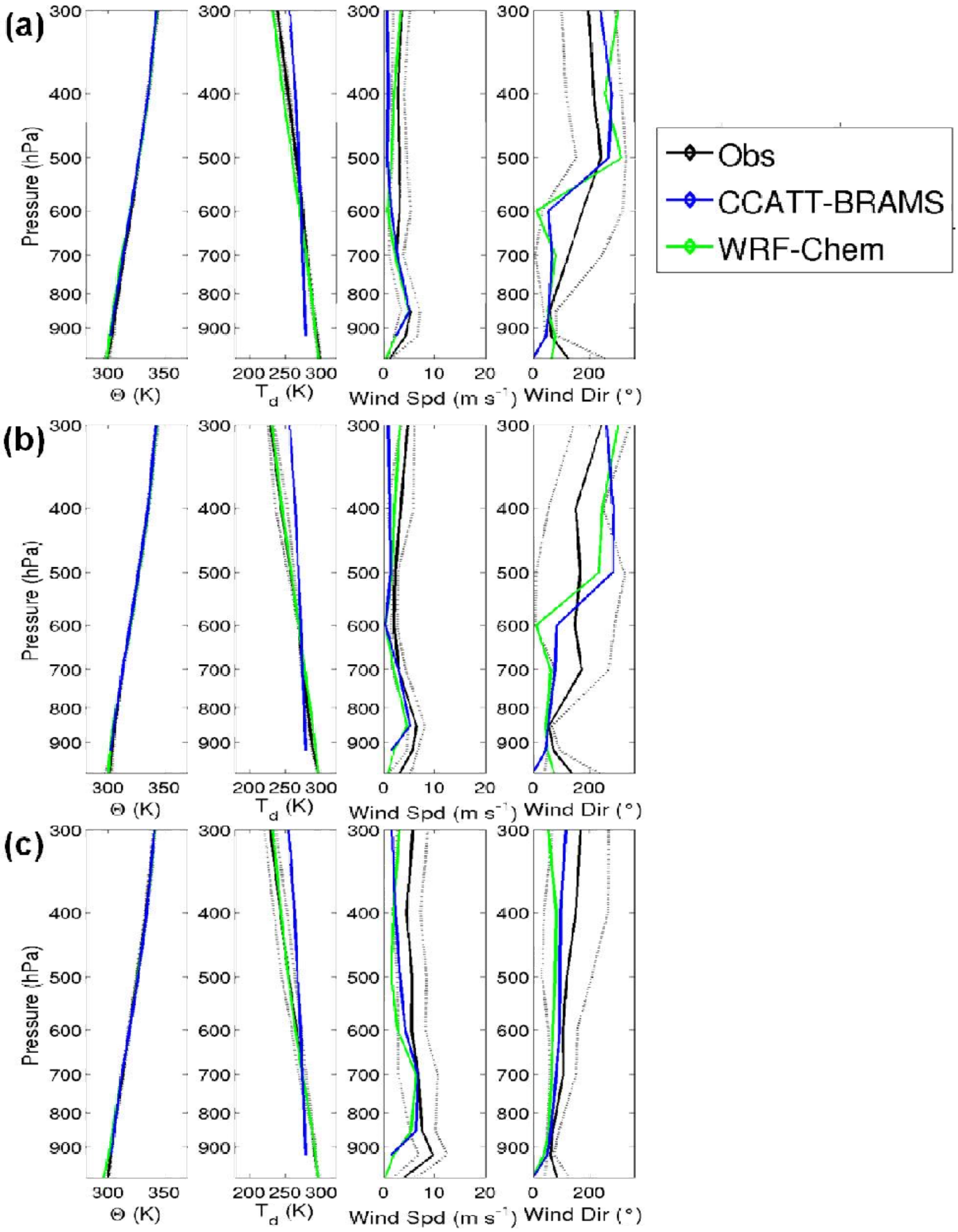

Figure 8. Mean vertical profiles at Manaus from radiosoundings (black, gray line denotes one standard deviation), CCATT-BRAMS (blue) and WRF-Chem (green) for October-November 2008 at (a) 0:00, (b) 12:00 and (c) 18:00 UTC.

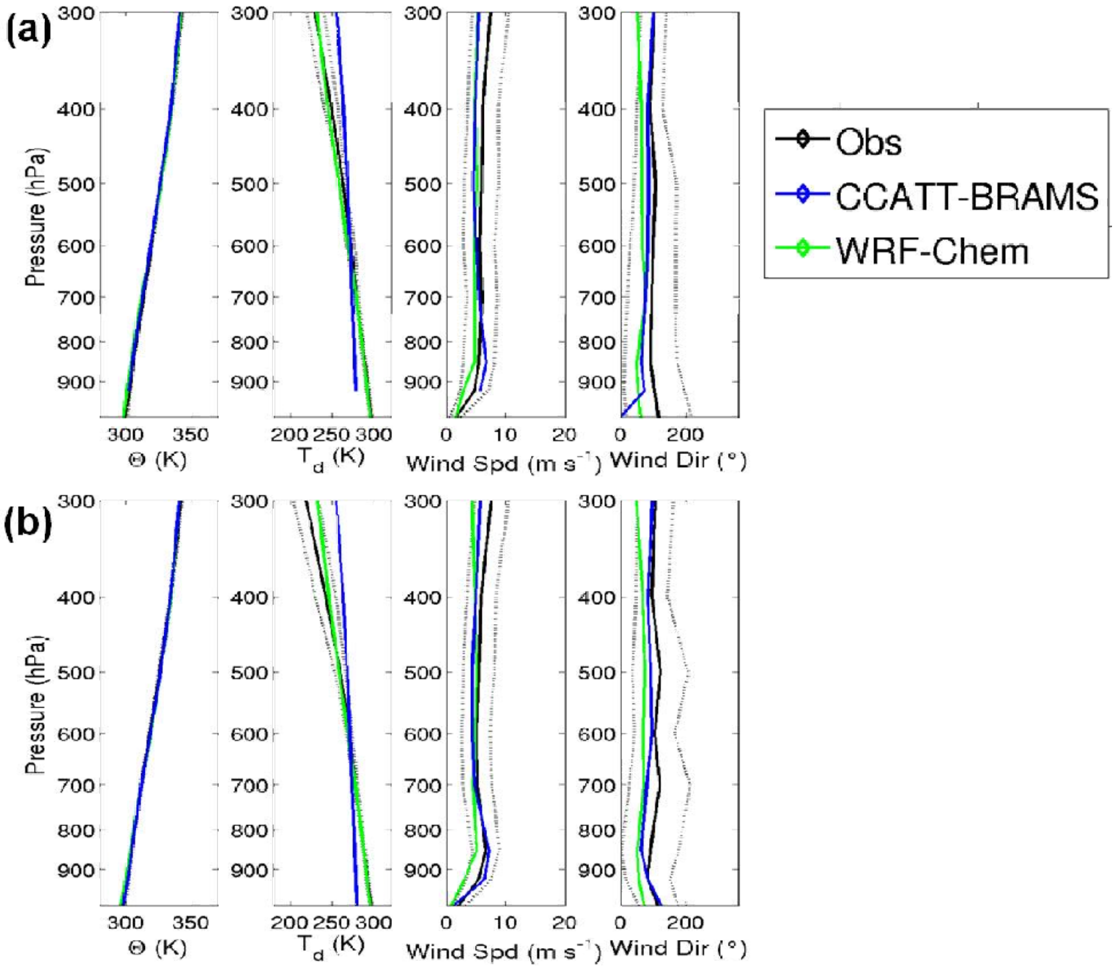

Figure 9. Mean vertical profiles at Manaus from radiosoundings (black, gray line denotes one standard deviation), CCATT-BRAMS (blue) and WRF-Chem (green) for April-May 2009 at (a) 0:00 and (b) 12:00 UTC.

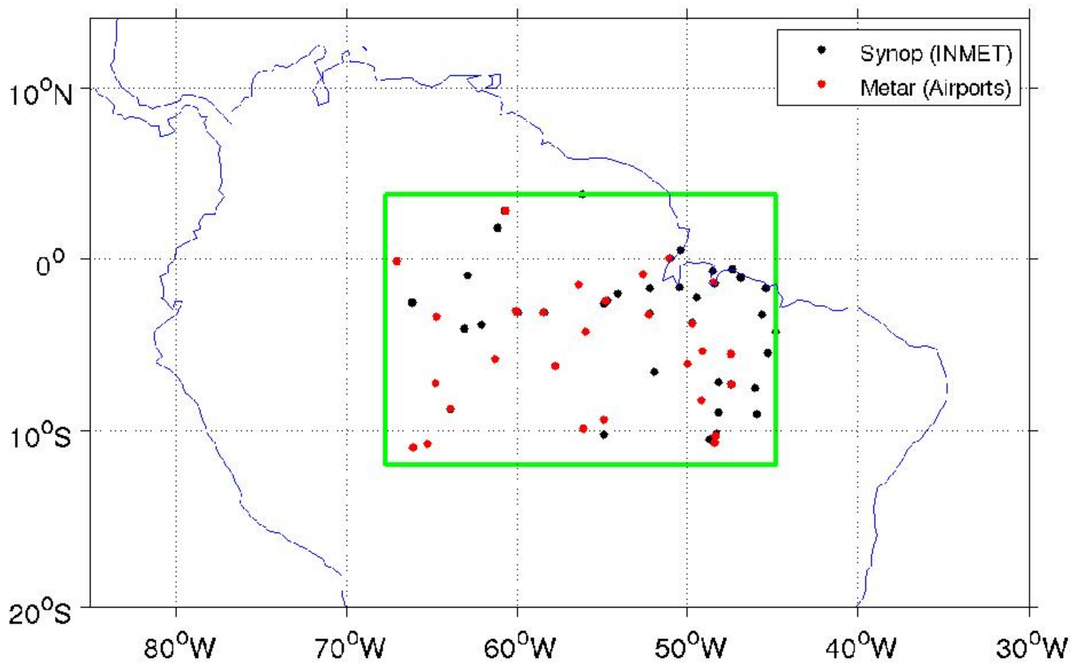

Figure 10. Locations of surface meteorological stations for model evaluation.

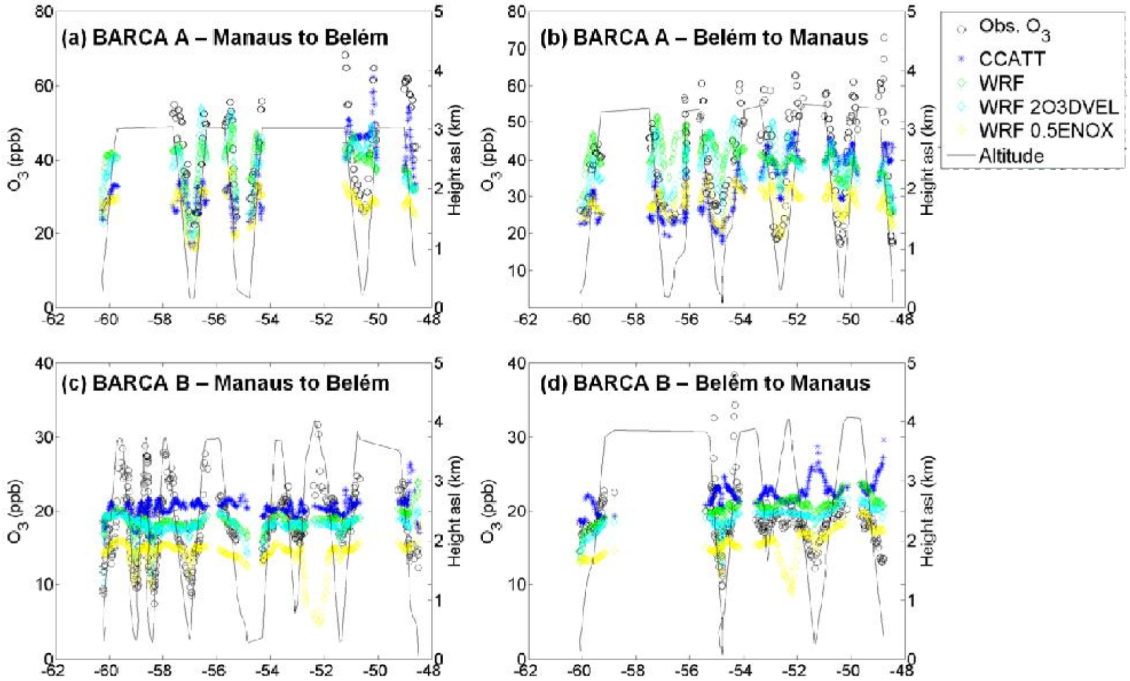

Figure 11. O_3 as observed (black circles) and simulated with CCATT-BRAMS (blue stars) and WRF-Chem (base case – green diamonds, 2DEPVEL – cyan circles and 0.5ENOx – yellow squares) from BARCA flights (a) from Manaus to Belém on 18 November 2008, (b) Belém to Manaus on 19 November 2008, (c) Manaus to Belém on 21 May 2009 and (d) Belém to Manaus on 23 November 2009.

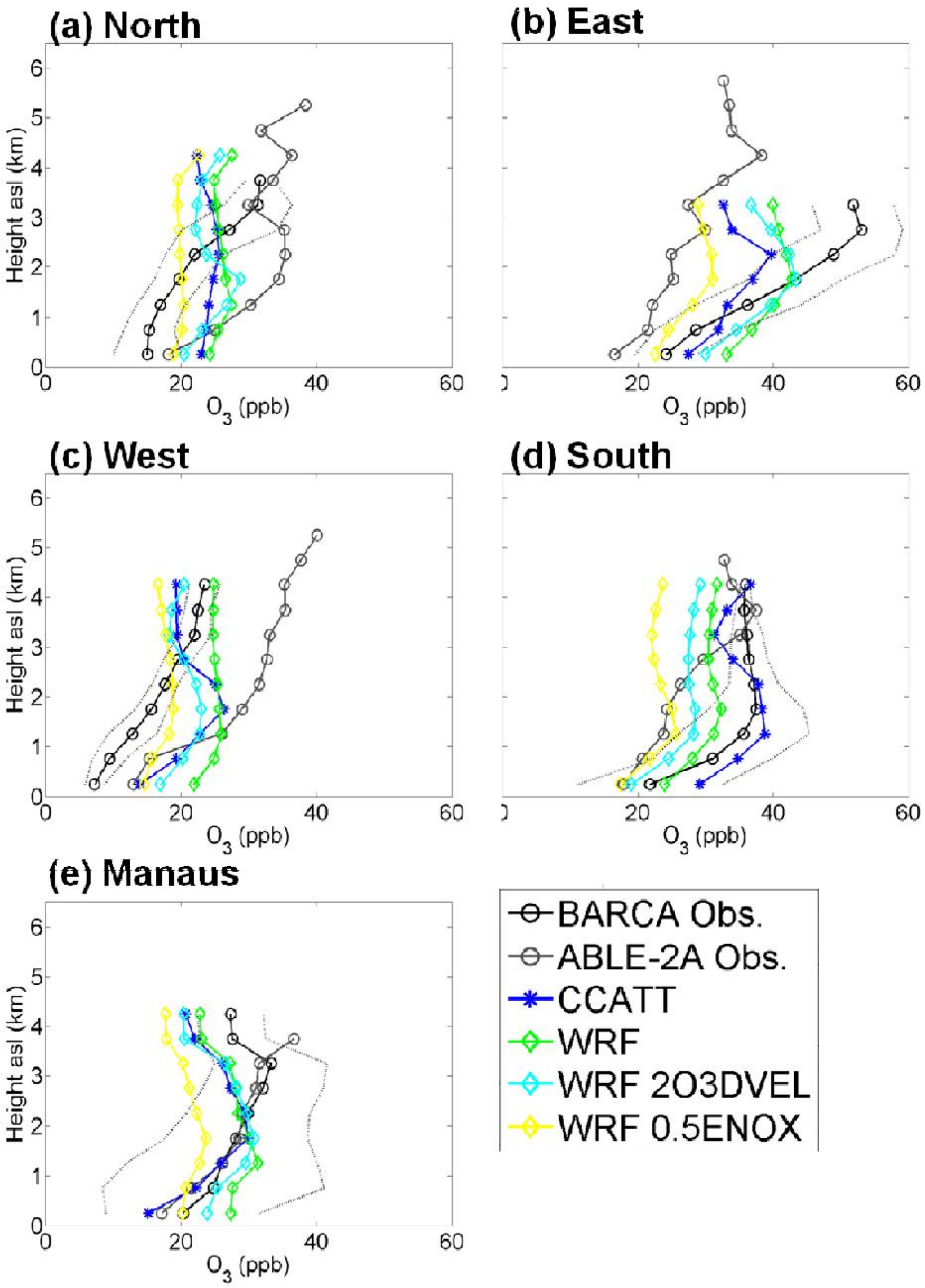

Figure 12. Mean vertical O_3 profiles for BARCA A flights for observations (black, gray line denotes one standard deviation), CCATT-BRAMS (blue) and WRF-Chem (base case – green, 2DEPVEL – cyan and 0.5ENOx – yellow) simulations by region: (a) north, (b) east, (c) west, (d) south and (e) around Manaus. ABLE-2A observations (gray) from the same regions are included for comparison.

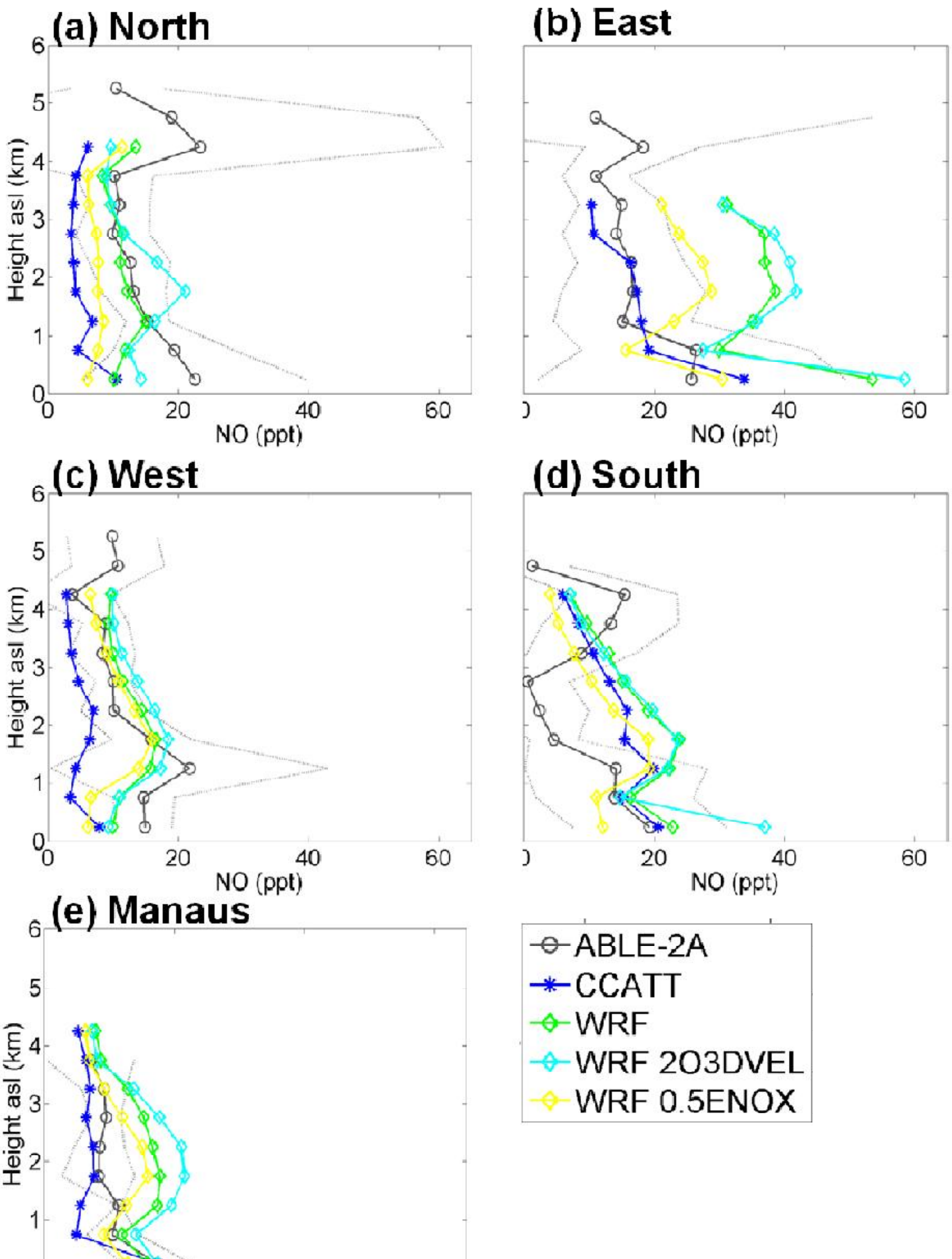

Figure 13. Mean vertical NO profiles corresponding to BARCA A flights for CCATT-BRAMS (blue) and WRF-Chem (base case – green, 2DEPVEL – cyan and 0.5ENOx – yellow) simulations by region: (a) north, (b) east, (c) west, (d) south and (e) around Manaus. ABLE-2A observations (gray) from the same regions are included for comparison.

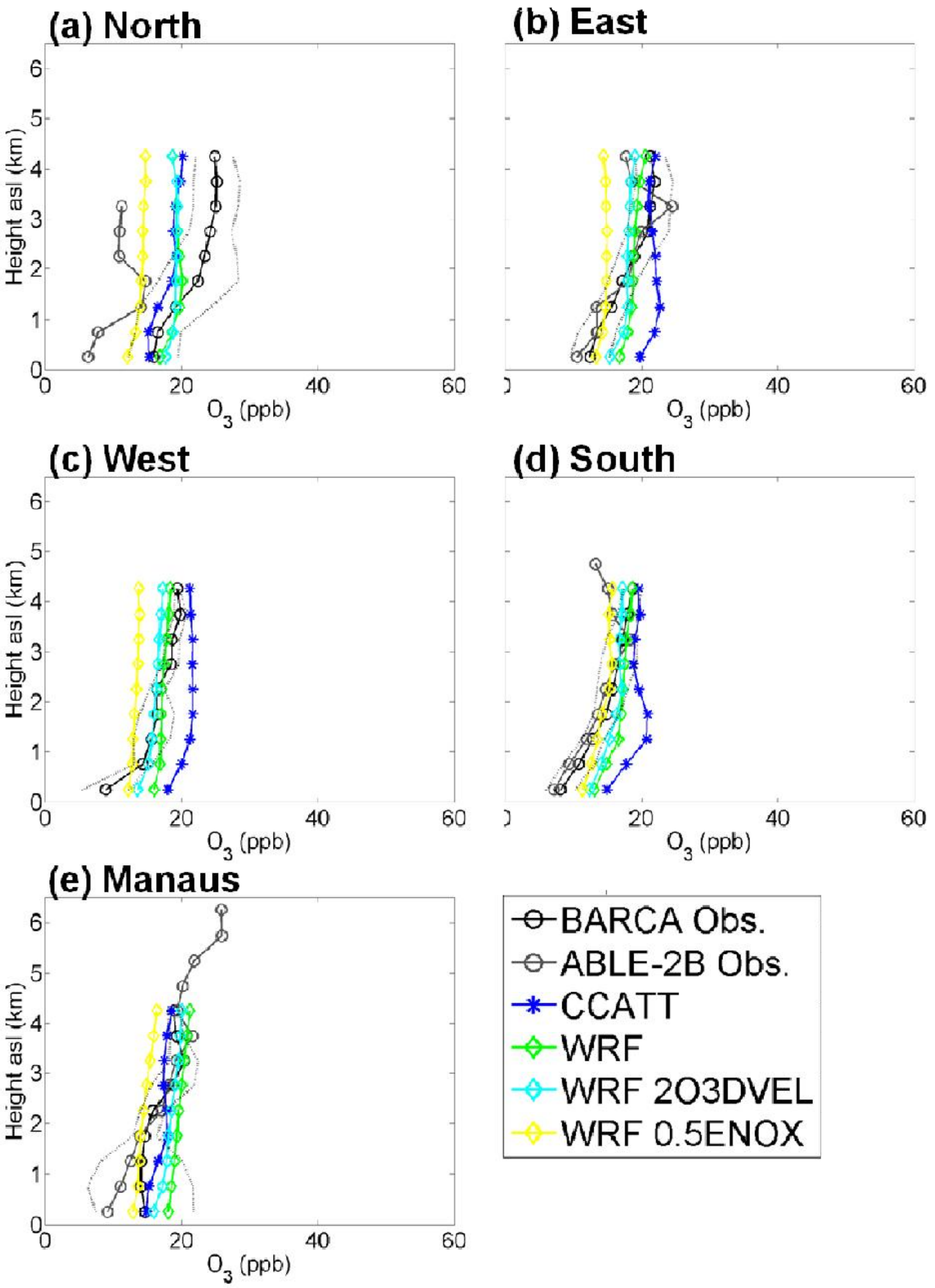

Figure 14. Mean vertical O_3 profiles for BARCA B flights for observations (black, gray line denotes one standard deviation), CCATT-BRAMS (blue) and WRF-Chem (base case – green, 2DEPVEL – cyan and 0.5ENOx – yellow) simulations by region: (a) north, (b) east, (c) west, (d) south and (e) around Manaus. ABLE-2A observations (gray) from the same regions are included for comparison.

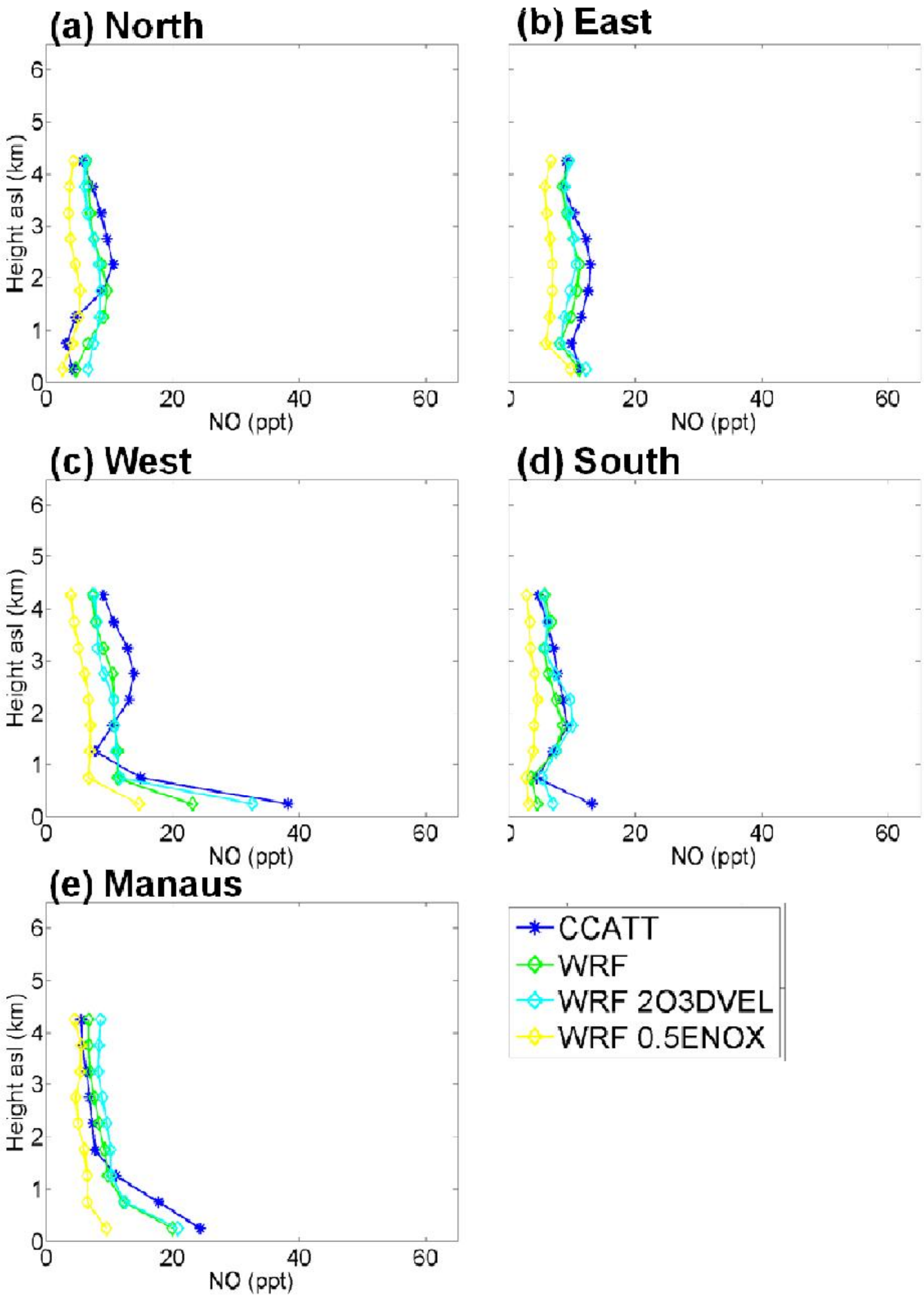

Figure 15. Mean vertical NO profiles corresponding to BARCA B flights for CCATT-BRAMS (blue) and WRF-Chem (base case – green, 2DEPVEL – cyan and 0.5ENOx – yellow) simulations by region: (a) north, (b) east, (c) west, (d) south and (e) around Manaus.

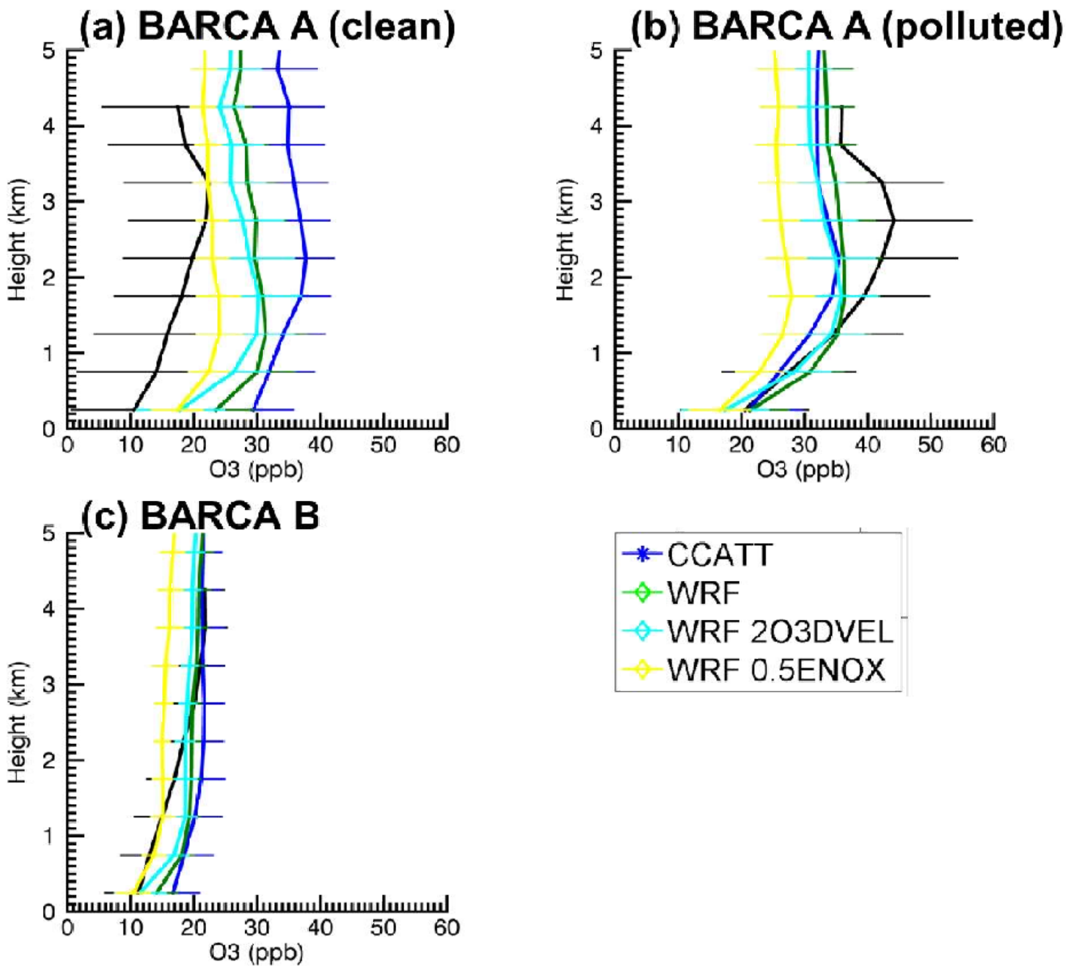

Figure 16. O_3 as observed (black circles) and simulated with CCATT-BRAMS (blue stars) and WRF-Chem (base case – green diamonds, 2DEPVEL – cyan circles and 0.5ENOx – yellow squares) during (a) BARCA A, clean conditions (west, north and around Manaus regions), (b) BARCA A, polluted conditions (east and south regions) and (c) BARCA B.

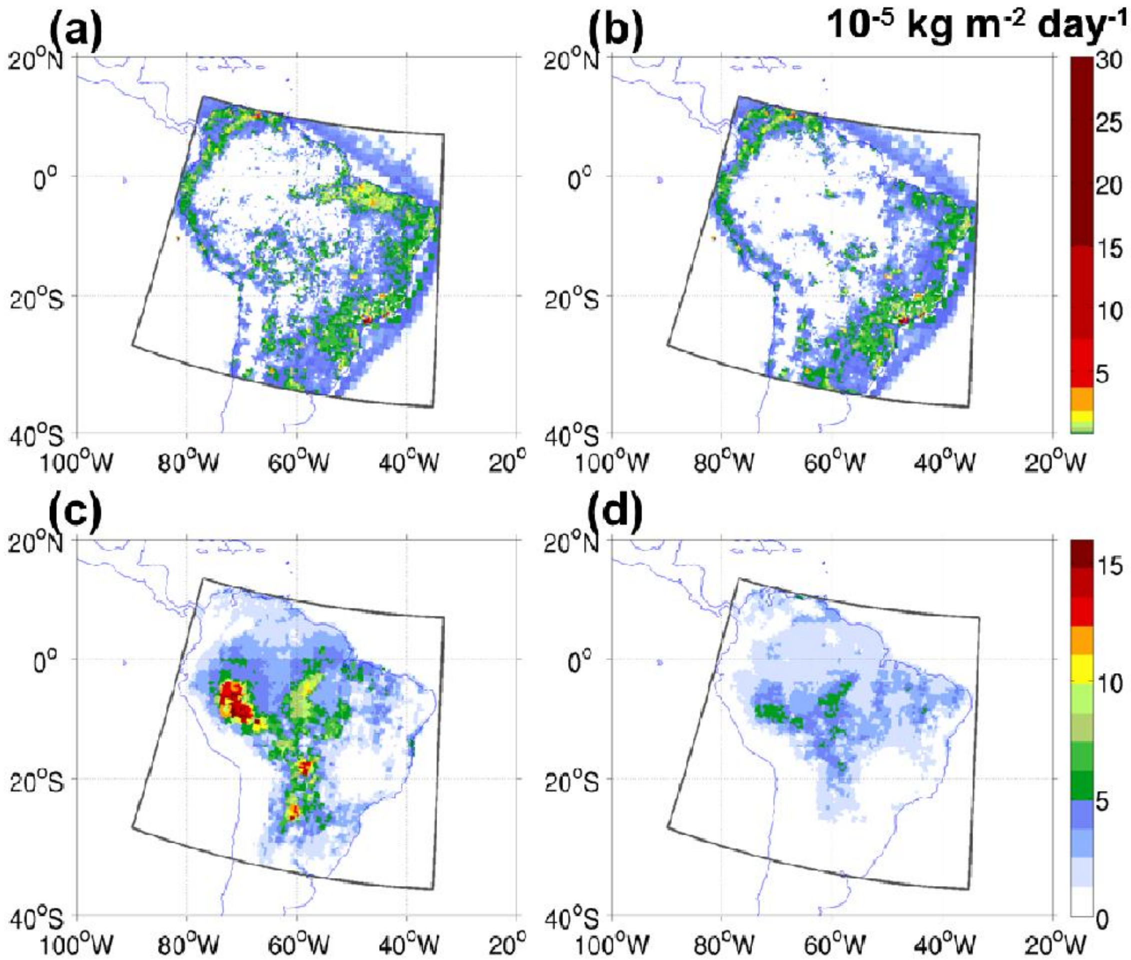

Figure 17. Mean emission rates (10^{-5} kg m^{-2} d^{-1}) from PREP-CHEM-SRC for the 35 km domain (dark gray outline) for NO_x for (a) BARCA A (November 2008) and (b) BARCA B (May 2009) and isoprene for (c) BARCA A and (d) BARCA B periods.

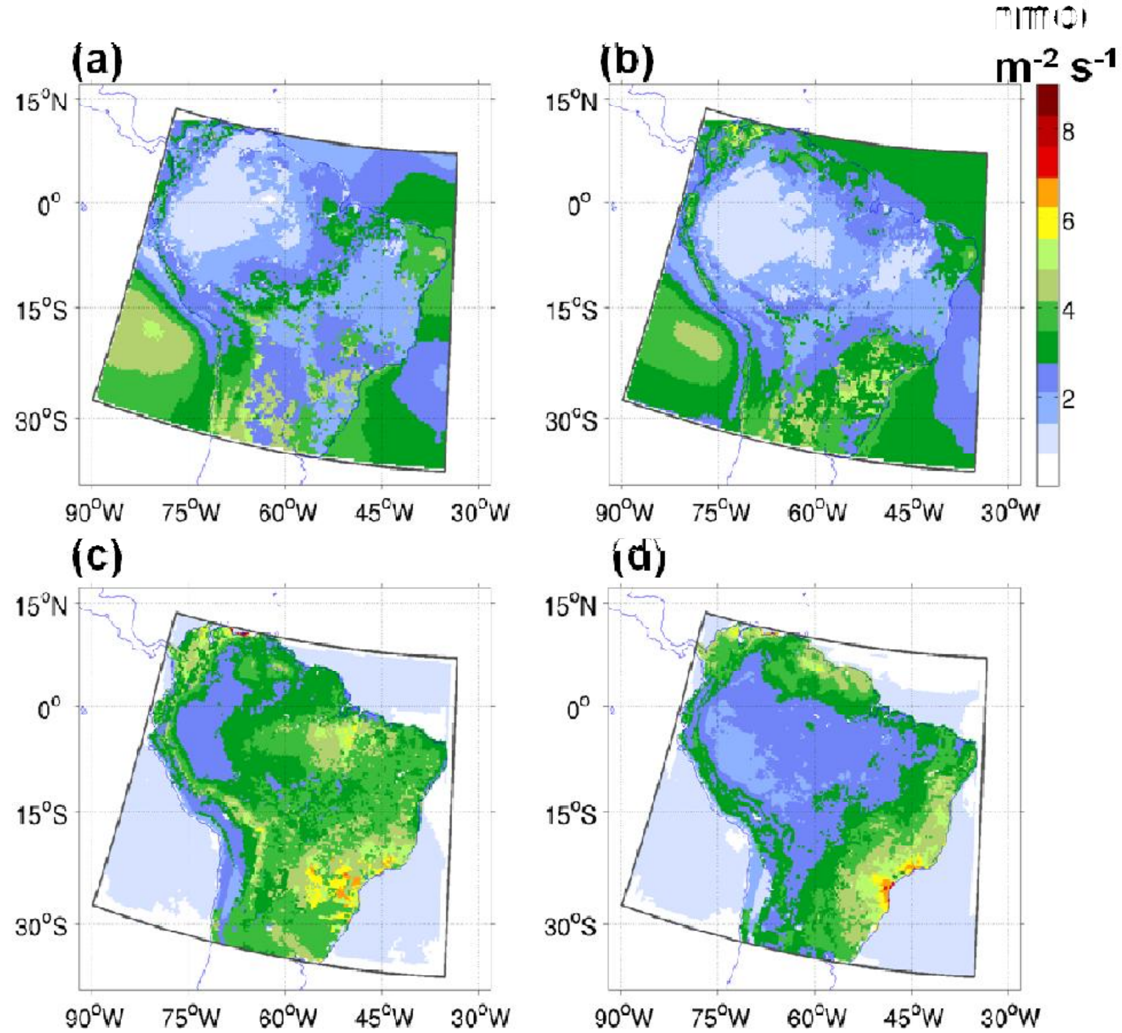

Figure 18. Average O_3 dry deposition flux (nmol m^{-2} s^{-1}) as simulated on the 35 km resolution domain (dark gray outline) by the CCATT-BRAMS model for (a) November 2008 and (b) May 2009 and by the WRF-Chem model for (c) November 2008 and (d) May 2009.

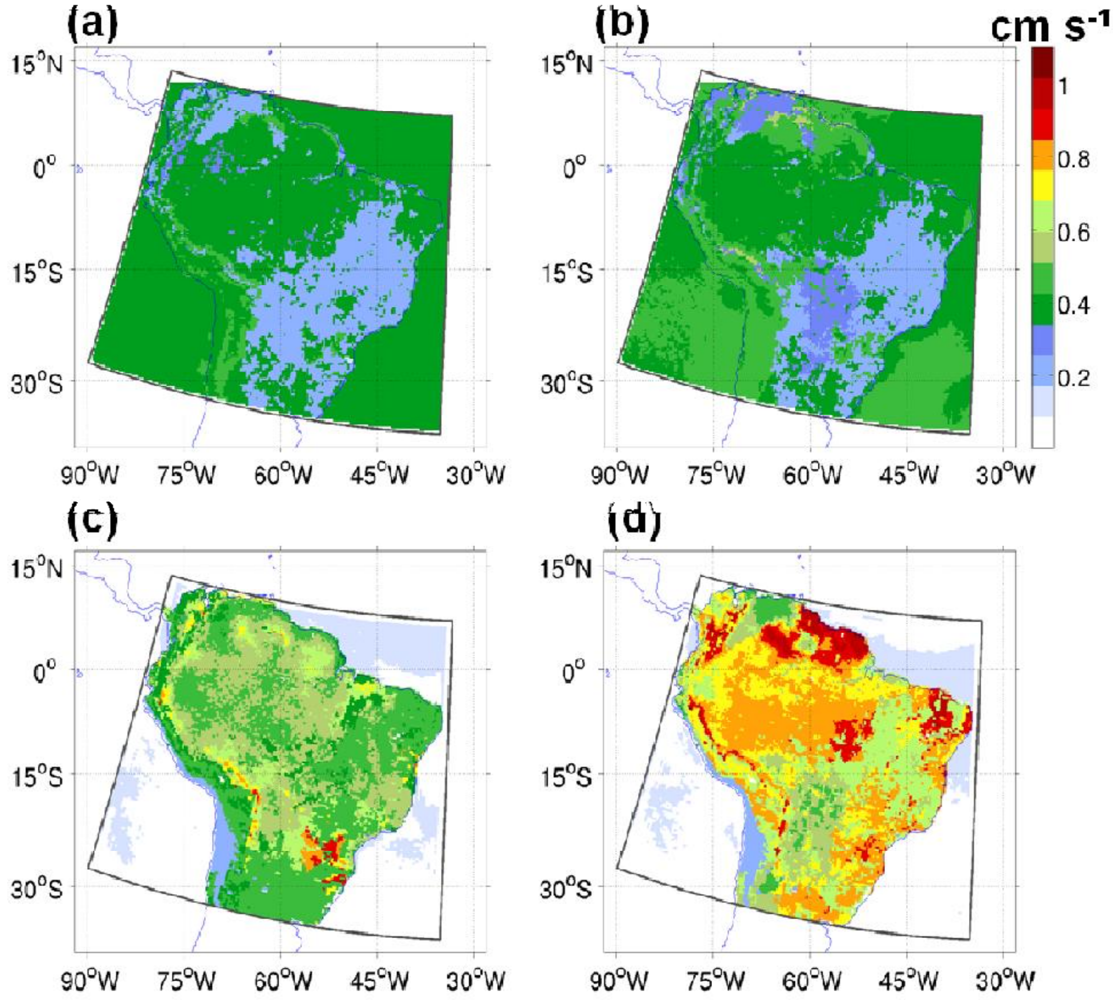

Figure 19. Same as Fig. 18, but daytime (11:00-21:00 UTC) median deposition velocity (cm s^{-1}).

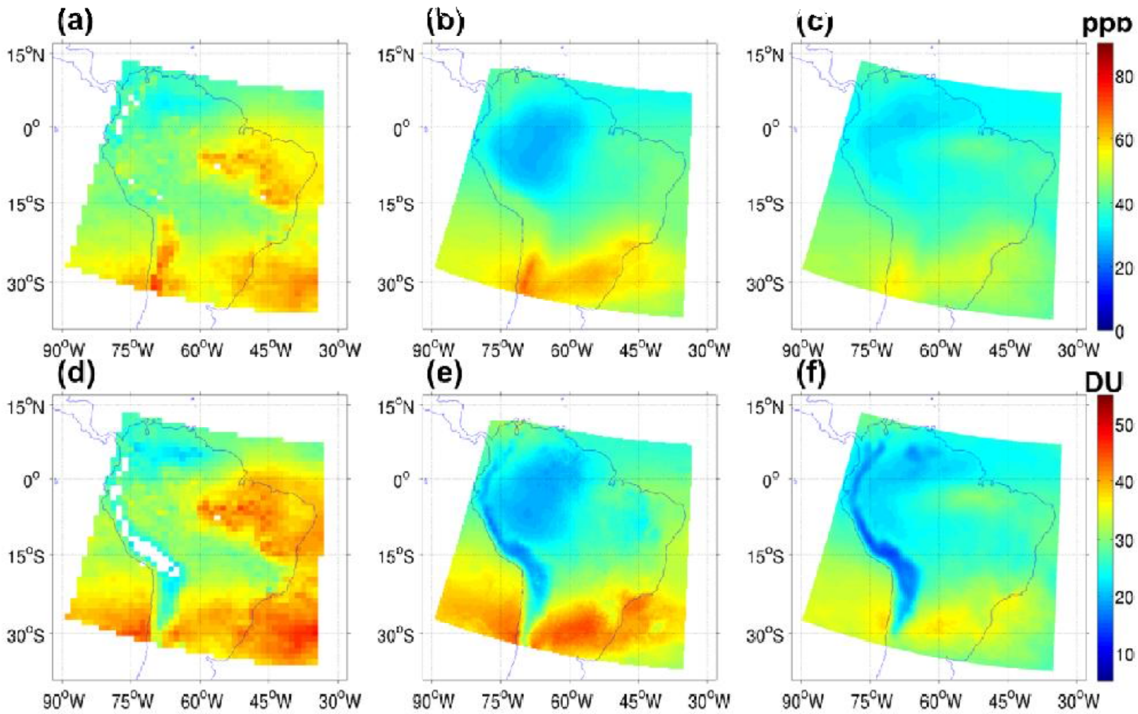

Figure 20. Mean tropospheric O_3 (ppb) on the 35 km domain from (a) OMI/MLS, (b) CCATT-BRAMS and (c) WRF-Chem and total tropospheric column O_3 (Dobson units) from (d) OMI/MLS, (e) CCATT-BRAMS and (f) WRF-Chem for November 2008.

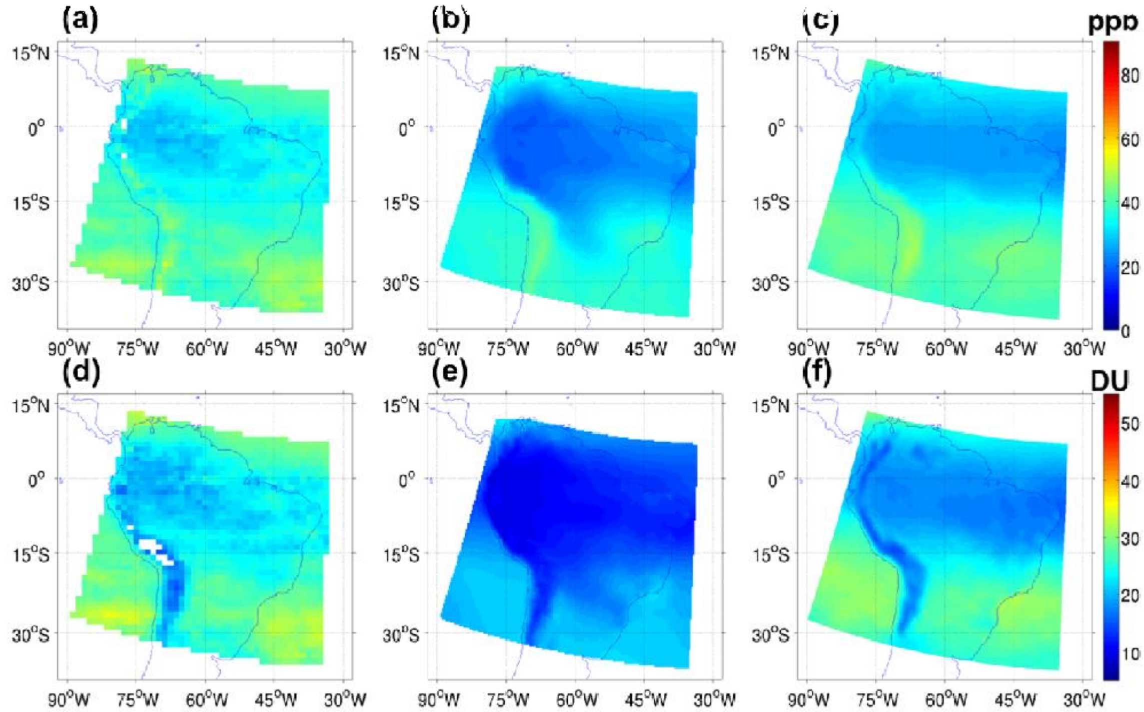

Figure 21. Same as Fig. 20, but for May 2009.

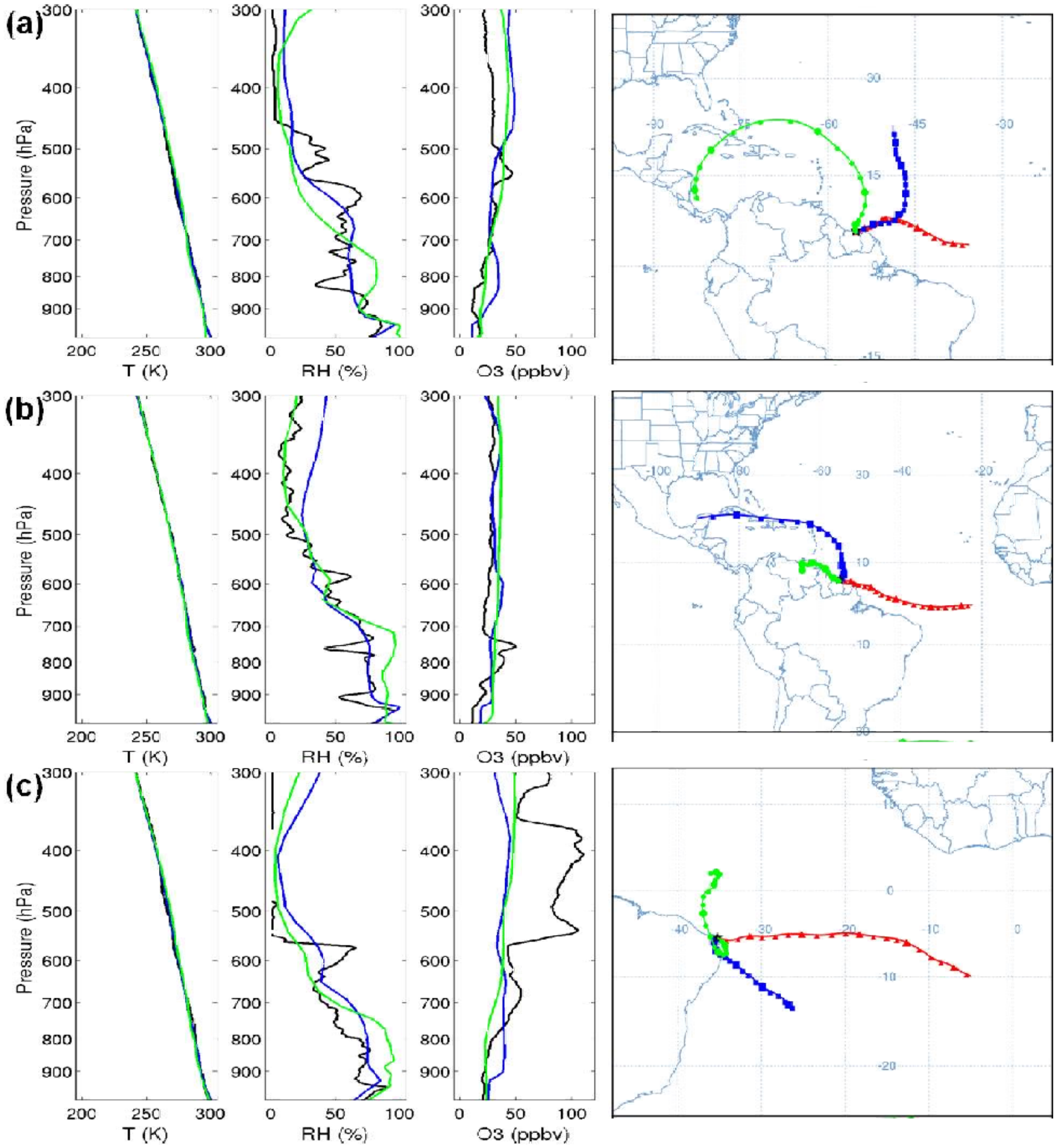
(a)
(b)
(c)
Pressure (hPa)
T (K)
RH (%)
O3 (ppbv)
300
400
500
600
700
800
900
200
250
0
50
100

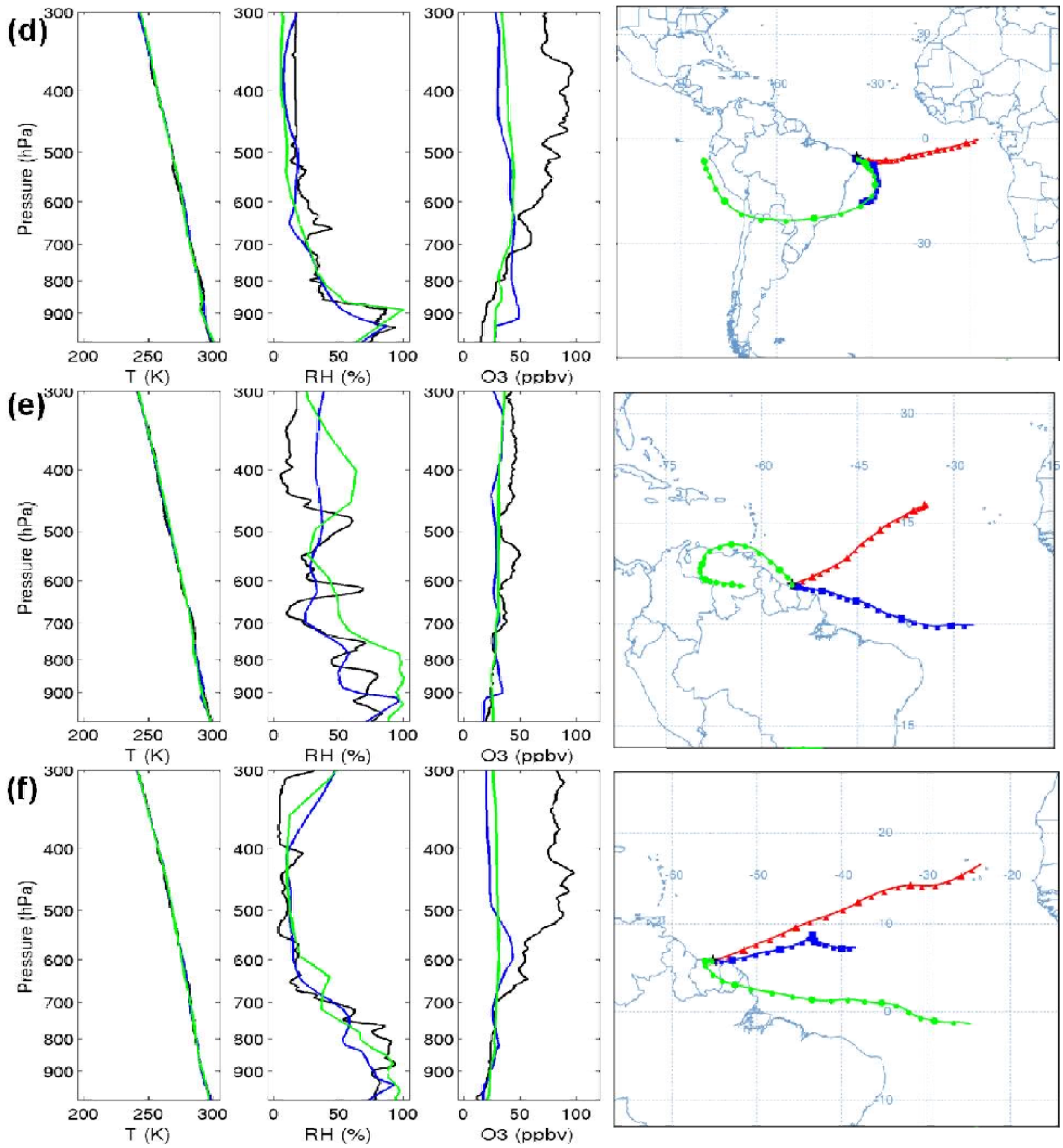

Figure 22. Vertical profiles of potential temperature, relative humidity, and O_3 from SHADOZ soundings (black), CCATT-BRAMS (blue) and WRF-Chem (green) and HYSPLIT back trajectories at 13:00 UTC at 1500 m (~850 hPa, red), 6000 m (~470 hPa, blue) and 9000 m (~310 hPa, green) for: Paramaribo on (a) 6 November and (b) 25 November 2008, Natal on (c) 7 November and (d) November 19 2008 and Paramaribo on (e) 4 May and (f) 11 May 2009.